In Situ Spectroscopic Investigation of the Molecular and Electronic Structures of SiO_2 Supported Surface Metal Oxides

Edward L. Lee and Israel E. Wachs*

Operando Molecular Spectroscopy and Catalysis Laboratory, Chemical Engineering Department, 111 Research Drive, Iacocca Hall, Lehigh University, Bethlehem, Pennsylvania 18015

Received: May 9, 2007; In Final Form: July 13, 2007

Groups 5−7 transition metal oxides (V_2O_5, Nb_2O_5, Ta_2O_5, CrO_3, MoO_3, WO_3, Re_2O_7) were anchored on a SiO_2 support via incipient wetness impregnation and calcination. The molecular and electronic structures of the dehydrated supported metal oxides and the SiO_2 support were determined by combined in situ Raman, IR, and UV−vis spectroscopy under dehydrated conditions. In situ Raman characterization reveals that the supported metal oxides are only present as surface species below the maximum dispersion limit (where crystalline metal oxide nanoparticles are absent). In situ IR analysis shows that the surface metal oxides anchor to the SiO_2 support at Si−OH and adjacent Si−O−Si sites. The corresponding in situ UV−vis diffuse reflectance spectroscopy indicates that the dehydrated surface metal oxide species are present as isolated structures. Isotopic D_2O-H_2O exchange demonstrates that the dehydrated surface MO*x* species possess the M═O oxo functionality but no M−OH bonds. The number of M═O oxo bonds was found to be related to the metal oxide oxidation state or group number. The group 5 surface metal oxides are present as surface monoxo O═M(−O−Si)$_3$ species. The group 6 surface metal oxides primarily contain the surface dioxo (O═)$_2$M(−O−Si)$_2$ structures with some surface monoxo O═MO_4 species also present. In situ Raman under reduction environments allowed for the discrimination between these multiple MO*x* surface species as well as between vibrations from the metal oxides and the silica support. Only rhenia from the group 7 surface metal oxides was examined and found to possess the surface trioxo (O═)$_3$Re−O−Si structure. These molecular and electronic structural insights for dehydrated surface metal oxides on SiO_2 catalysts will facilitate the establishment of fundamental structure−activity relationships for future catalytic reaction studies.

1. Introduction

Supported metal oxide catalysts consist of highly dispersed metal oxides, that are the catalytic active sites for numerous reactions, on the surface of oxide supports (SiO_2, Al_2O_3, TiO_2, etc.).[1−3] Below monolayer surface coverage or maximum dispersion limit, the supported metal oxide phase can be present as a two-dimensional surface metal oxide layer that is 100% dispersed on the support. The dispersion of the supported metal oxide layers on SiO_2, however, is generally less than 100% because of the lower reactivity and greater acidic character of the silica surface hydroxyls.[4] The high surface area, excellent thermal/mechanical stability, and inexpensive cost of SiO_2 support materials have led to the wide industrial utilization of SiO_2-based supports: alkane oxidative dehydrogenation over supported V_2O_5/SiO_2 catalysts,[5−9] ethylene polymerization over supported CrO_3/SiO_2 catalysts,[10−12] selective catalytic reduction of NO with ammonia and selective oxidation of methane over supported MoO_3/SiO_2 catalysts,[4,13,14] and olefin metathesis over supported WO_3/SiO_2 and Re_2O_7/SiO_2 catalysts.[15] The extensive interest in silica-supported catalysts has motivated many investigations into developing synthesis methods that enhance the dispersion of metal oxides on silica supports.[16−18] In addition, SiO_2 supported metal oxide catalysts represent model catalytic systems that can allow for the development of fundamental structure−activity relationships because the surface metal oxides are 100% dispersed at low metal oxide loadings.

It is important to determine the molecular and electronic structures of the surface metal oxide catalytic active sites in order to (i) obtain insights into the fundamental factors affecting the reactivity and selectivity of the catalytic active sites and to (ii) be able to improve their catalytic properties for specific applications. The catalytic active metal oxide species anchor to the SiO_2 substrate via titration of the surface hydroxyls, which results in the dispersed two-dimensional surface overlayer. The anchored dehydrated surface metal oxide structure can terminate with either M−O$^-$, M−OH, M−O−M, or M═O functionalities.[19−23] The dehydrated group 5, 6, and 7 transition metal oxides supported on SiO_2 yield unique structures since they have been claimed to terminate with monoxo (M═O), dioxo (M(═O)$_2$), or trioxo (M(═O)$_3$) functionalities.[23] Coupled Raman and infrared (IR) spectroscopy have been used to try to determine the number of terminal M═O bonds present in surface metal oxide structures.[24] Raman spectroscopy readily provides the vibrations of the supported metal oxide species on SiO_2 because of the relatively weak bands from the SiO_2 support.[2,3] IR spectroscopy, unfortunately, tends to only provide a small window from ∼850−1000 cm^{-1} for silica-supported metal oxides because of the strong IR absorbance by the SiO_2 support below ∼850 cm^{-1} and above ∼1000 cm^{-1}.[3] The vibrations of the dehydrated surface metal oxide species, however, can sometimes be detected in the vibrational overtone region (∼1900−2100 cm^{-1}). Corresponding UV−vis diffuse reflectance spectroscopy (DRS) provides the local structure (isolated monomer, dimer, polymeric chain, cluster, or three-dimensional

* Corresponding author. E-mail: iew0@lehigh.edu. Phone: (610) 758-4274. Fax: (610) 758-6555.

10.1021/jp0735482 CCC: $37.00
Published on Web 09/12/2007

(3D) structure) of the catalytic active metal oxide cation via ligand-to-metal charge transfer (LMCT) band position and the corresponding edge energy (Eg) value.[2,23] Although progress has been made in recent years in the characterization of SiO_2 supported metal oxide catalysts under different environments through spectroscopic studies, there still remain many unresolved structural questions and inconsistencies in the literature that need to be addressed (e.g., definitive determination of the molecular and electronic structures of the dehydrated surface MO*x* species on SiO_2).

A critical molecular structural issue is the number of terminal metal oxo bonds contained in the surface metal oxide species on SiO_2 under dehydrated conditions. In general, monoxo M═O structures only give rise to one symmetric (υ_s) vibration; dioxo M(═O)$_2$ structures give rise to both symmetric (υ_s) and asymmetric (υ_{as}) bands that are separated by ~10−30 cm^{-1},[24,25] and trioxo M(═O)$_3$ structures exhibit one symmetric and several associated asymmetric bands. In addition, the bond order of terminal M═O functionalities in gas-phase oxyhalide complexes decreases with the number of oxo bonds (M═O > M(═O)$_2$ > M(═O)$_3$), and decreasing the M═O bond order shifts the vibration to lower wavenumber values. It is, however, not straightforward to predict the exact location of vibrations for the silica-supported metal oxide species from gaseous oxyhalides since the halide ligands affect the exact vibrational position of the oxo functionalities.

The vibrations of halide-free oxo complexes, however, more accurately reflect the exact vibrations of supported metal oxide species [e.g., Keggin $H_3SiM_{12}O_{40}$ clusters that contain monoxo functionality (Mo═O (1006 cm^{-1}), W═O (1022 cm^{-1}), and V═O (1034 cm^{-1})),[26] gas-phase Re_2O_7 dimer (Re(═O)$_3$ at 1009 (υ_s)/972 (υ_{as}) cm^{-1}), and silsesquioxane compounds (monoxo $(Ph_3SiO)_3V$═O with V═O at 1022 cm^{-1} and dioxo $(Ph_3SiO)_2$Cr(═O)$_2$ with O═Cr═O at 985 (υ_s)/1014 (υ_{as}) cm^{-1})].[27,28] Density functional theory (DFT) calculations have recently been performed for the groups 5 and 6 metal oxides on silica that can further aid in the discrimination between monoxo and dioxo species. The monoxo V═O vibration is predicted to be at 1038−1047 cm^{-1} for VO_4 species from DFT calculations.[29,30] The DFT calculations predict that the monoxo Cr═O vibration of CrO_5 species will occur at 1033 cm^{-1} and that the dioxo (O═Cr═O) vibration of CrO_4 species will be found at 983 (υ_s)/1010 (υ_{as}) cm^{-1}.[31] The DFT calculations for monoxo Mo═O species predict a band at 1014 cm^{-1} and for dioxo (O═Mo═O) species predict a band at 995 (υ_s)/977 (υ_{as}) cm^{-1}.[32] DFT calculations for supported WO_3/SiO_2 have not appeared in the literature; however, by similarity with molybdena, monoxo W═O is expected to vibrate at ~1020 cm^{-1}, and dioxo O═W═O is expected to vibrate at ~998 (υ_s)/~972 (υ_{as}) cm^{-1}. The vibrations of a comprehensive set of metal oxo reference structures are summarized in Table 1 and will be used to assist in the surface metal oxide structural assignments of this paper.

The objective of the present study is to fully characterize and definitively determine the molecular and electronic structures of the dehydrated surface VO*x*, NbO*x*, TaO*x*, CrO*x*, MoO*x*, WO*x*, and ReO*x* species on SiO_2 with the aid of in situ Raman, IR, and UV−vis spectroscopy under oxidizing (O_2) and reducing (H_2) conditions and D_2O/H_2O exchange. First, unlike previous in situ Raman studies primarily employing only visible excitation, the Raman spectrum of each dehydrated silica-supported MO*x* catalytic system is examined with multiple excitations (532, 442, and 325 nm). The use of multiple laser excitations allows for elimination of sample fluorescence that sometimes plagued earlier Raman measurements and provides for possible resonance enhancement of weak Raman bands that may not have been detected in earlier studies.[33−35] The Raman spectra with the clearest band distinction or best resolution from one of these laser lines are presented in this paper for each system, and the comparison of the effect of different laser excitation energies will be detailed in a subsequent paper. Second, the reducibility for each dehydrated surface MO*x* species is examined by exposing the catalysts to H_2 environments at elevated temperatures. Partial reduction of surface metal oxides can discriminate between vibrational modes of multiple sites because of their generally differing reduction characteristics (selective reduction). The decoupling of vibrational bands can also be established if multiple vibrations are found to have different rates of reduction during time-resolved spectroscopy. In such studies where the catalyst samples become darker upon reduction, the vibrations of the SiO_2 support (487, 605, and 800 cm^{-1}) can be employed as internal intensity standards since the silica support does not reduce. Third, isotopic H_2O-D_2O exchange studies are also performed to properly assign vibrational bands arising from H-containing functionalities (e.g., Si−OH, M−OH, etc.), which should give rise to shifting of band positions during the H_2O-D_2O exchange. Fourth, the local surface MO*x* electronic structures are also examined with in situ UV−vis DRS under dehydrated, oxidized conditions. Silica is used as the UV−vis baseline and reflectance standards since it does not exhibit absorbance in the UV to visible region. This comprehensive characterization of the different silica supported surface MO*x* systems with the same instrumentation allows, for the first time, the complete structural determination of the dehydrated surface MO*x* species on SiO_2. The fundamental structural information can be employed in subsequent studies to establish molecular/electronic structure−activity/selectivity relationships for SiO_2 supported metal oxide catalysts.

2. Experimental Methods

2.1. Catalyst Synthesis and Preparation. Amorphous SiO_2 (Cabot, Cab-O-Sil fumed silica EH-5, S.A. = 332 m^2/g) was employed as the silica support material and was found to be more easily handled by an initial water pretreatment and calcination at 500 °C without changing the material properties.[36−38] The highly dispersed silica-supported metal oxide catalysts were successfully prepared by incipient wetness impregnation of aqueous and nonaqueous solutions of the corresponding reactive H-sequestering precursors: vanadium triisopropoxide[36] (VO[CHO(CH$_3$)$_2$]$_3$, Alfa Aesar, 97%), niobium ethoxide[37,39] (Nb(OC$_2$H$_5$)$_5$, Alfa Aesar, 99.999%), tantalum ethoxide[40] (Ta(OC$_2$H$_5$)$_5$, Alfa Aesar, 99.999%), chromium(III) nitrate[41,42] (Cr(NO$_3$)$_3$·9H$_2$O, Alfa Aesar, 98.5%), ammonium heptamolybdate[43] ((NH$_4$)$_6$Mo$_7$O$_{24}$·4H$_2$O, Aldrich, 99.98%), ammonium metatungstate[44] ((NH$_4$)$_6$H$_2$W$_{12}$O$_{40}$·*x*H$_2$O, Pfaltz and Bauer, 99.5%), and perrhenic acid[45,46] (HReO$_4$, Alfa Aesar, 75−80%). The nonaqueous preparations of the organic precursors were carried out in a glovebox (Vacuum Atmospheres, Omni-Lab VAC 101965) under N_2 environment using an incipient wetness point of ~1.2 mL/g SiO_2 with a toluene solvent, while the aqueous preparations were synthesized in ambient conditions with an incipient wetness point of ~0.9 mL/g SiO_2. The samples were allowed to dry overnight followed by a second drying step, both drying steps under their respective gas environments, holding the samples at 110 °C for 2 h in a programmable furnace (Thermolyne, Model 48000). Finally, all of the synthesized catalysts were subjected to calcination by ramping the temperature at 1 °C/min under flowing air (Airgas, Zero grade) to 500 °C (in keeping with earlier studies, 450 °C was employed

TABLE 1: Summary of Metal Oxo Vibrations of Gas-Phase Metal Oxyhalides, Bulk Metal Oxides, Dehydrated Keggin Clusters, Silsesquioxane Reference Compounds, and Metal Oxo Vibrations Based on DFT/ab Initio Calculations

metal oxide oxo structure	reference compound	ν_s(M═O)/ν_{as}(M═O) (cm^{-1})
V compounds		
monoxo	$X_3V{=}O$	1025−1058 (X = Br < Cl < F)[63,102]
monoxo	$(Si{-}O)_3V{=}O$	1038−1047[c,29,30,65]
monoxo	$H_3SiMo_{11}V_1O_{40}$	1034[b]
monoxo	$(Ph_3SiO)_3V{=}O$	1022[a]
dioxo	$[F_2V(=O_2)]^-$	970/962[102]
dioxo	$[Cl_2V(=O_2)]^-$	970/959[102]
Nb compounds		
monoxo	$Cl_3Nb{=}O$	997
dioxo	$[S_2Nb(=O)_2]^{3-}$	897/872
Ta compounds		
monoxo	$Cl_3Ta{=}O$	∼950[d,23]
dioxo	$[S_2Ta(=O)_2]^{3-}$	∼800−860[d,23]
Cr compounds		
monoxo	$(Al{-}O)_4Cr{=}O$	1033[c,31]
monoxo	$F_4Cr{=}O$	1028[103]
dioxo	$F_2Cr(=O)_2$	1006/1016
dioxo	$(Ph_3SiO)_2Cr(=O)_2$	985/1014[a]
dioxo	$Cl_2Cr(=O)_2$	984/994[104]
dioxo	$(Si{-}O)_2Cr(=O)_2$	983/1010[a,31]
dioxo	CrO_3	975/1003[41]
trioxo	$CsBrCr(=O)_3$	908 (ν_s)/(933, 947, 955)(ν_{as})[105]
Mo compounds		
monoxo	$X_4Mo{=}O$	1008−1048 (X═Cl < F)[102]
monoxo	$(Si{-}O{-})_4Mo{=}O$	1014−1017[c,32]
monoxo	$H_3SiMo_{12}O_{40}$	1006[b]
dioxo	$Cl_2Mo(=O)_2$	997/971[32,102]
dioxo	$Br_2Mo(=O)_2$	995/970
dioxo	$(Si{-}O{-})_2Mo(=O)_2$	995/977[c,32]
W compounds		
monoxo	$X_4W{=}O$	1010−1055 (X = Br[d] < Cl[d] < F)[23,102]
monoxo	$H_3SiW_{12}O_{40}$	1022[b]
monoxo	$(Si{-}O{-})_4W{=}O$	1020[d]
dioxo	$(Si{-}O{-})_2W(=O)_2$[d]	998/972[d]
dioxo	$Cl_2W(=O)_2$	998/972[d]
Re compounds		
monoxo	$F_5Re{=}O$	990[106]
dioxo	$F_3Re(=O)_2$	1026/990[107]
trioxo	$XRe(=O)_3$	994−1013/963−978 (X = Br < Cl < F)[102]
trioxo	$O[Re(=O)_3]_2$ gas-phase dimer	1009/972[23]

[a] Silsesquioxanes compounds (Raman spectroscopy at 514.5 nm). [b] Heteropolyoxo anion Keggins (dehydrated, Raman spectroscopy at 514.5 nm). [c] Theoretical ab initio/DFT calculations. [d] Estimated values.

for supported V_2O_5/SiO_2) for 6 h. The final synthesized catalysts are denoted as V_2O_5/SiO_2, Nb_2O_5/SiO_2, Ta_2O_5/SiO_2, CrO_3/SiO_2, MoO_3/SiO_2, WO_3/SiO_2, and Re_2O_7/SiO_2.

The Ta− and W−silica xerogel samples were prepared following the procedure previously employed for synthesis of vanadia and chromia silica xerogels.[47,48] These xerogel samples, in addition to the Keggin $H_3SiM_{12}O_{40}$ cluster compounds, were spectroscopically measured under the same conditions used to monitor the dehydrated supported MOx/SiO_2 catalysts.

2.2. In Situ Raman Spectroscopy. The Raman spectra of the silica-supported metal oxide catalysts were obtained by a high resolution, dispersive Raman spectrometer system (Horiba-Jobin Yvon LabRam HR) equipped with three laser excitations (532, 442, and 325 nm). The visible laser at 532 nm (green) was generated by a Coherent Compass 315M-150, Nd:YAG double diode pumped laser (output power of 150 mW, sample power of 10 mW) while the visible laser at 442 nm (violet) and the UV laser at 325 nm (not visible) were generated by a He−Cd laser (Kimmon, model IK5751I-G; 441.6 nm output power of 110 mW, sample power of 28 mW; 325.0 nm output power of 30 mW, sample power of ∼7 mW). The lasers were focused on the samples with a confocal microscope equipped with a 50X long working distance objective (Olympus BX-30-LWD) for the visible lasers and 15X objective (OFR LMU-15X-NUV) for the UV laser. The LabRam HR spectrometer was optimized for the best spectral resolution by employing a 900 groves/mm grating (Horiba-Jobin Yvon 51093140HR) for the visible lasers and a 2400 grooves/mm grating (Horiba-Jobin Yvon 53011140HR) for the UV laser. The resolution for both gratings is ∼2 cm^{-1}. Specifically, the optimal resolution, or minimum number of data points required to resolve a peak, is based on the grating and laser excitation energy, where, for the 900 grating, the achievable resolution is 1.88 cm^{-1} (532 nm) and 2.76 cm^{-1} (442 nm), and for the 2400 grating, it is 1.76 cm^{-1} (325 nm). The Rayleigh scattered light was rejected with holographic notch filters (Kaiser Super Notch). The notch filter window cutoffs were ∼100 cm^{-1} for the visible lasers and ∼300 cm^{-1} for the UV laser. The scattered light, after removing the Rayleigh scattering, was directed into a UV-sensitive liquid N_2 cooled CCD detector (Horiba-Jobin Yvon CCD-3000V). The calibration of each laser line was performed with a Hg lamp by adjusting the groove gratings to match the zero position and minimize the error of the linearity across the full Raman spectrum range. The Hg lines chosen to represent the 532, 442, and 325 nm lasers were 546.07, 435.84, and 365.02 nm, respectively. Additionally, wavenumber calibration of the Raman spectrograph was checked using the silicon line at 520.7 cm^{-1}.

The catalyst samples, typically consisting of between 5 and 10 mg of loose powder, were placed in an environmentally

controlled high-temperature cell reactor (Linkam TS1500) containing a quartz window and O-ring seals that were cooled by cooling water. The sample temperature was controlled by a temperature controller (Linkam TMS94), providing linear heating rates of over 50 °C/min through an S-type thermocouple (Pt 10% Rh/Pt, accuracy of 1.5 °C from 0 to 1450 °C). However, the sample bed temperature was calibrated externally with a secondary thermocouple (K type: Ni−Cr/Ni−Al, accuracy of 2.2 °C from −200 to 1250 °C). The true bed temperature (Y) versus controller output temperature (X) is corrected and linearly follows $Y = 0.88X$. The Linkam TS1500 has capabilities of heating the sample to 1500 °C with a maximum working gas flowrate of 60 sccm. Typical reactor cell conditions were 450−700 °C, 10−30 °C/min heating and cooling rates, atmospheric pressure, and ∼30 sccm gas flowrates metered by mass flow controllers (Brooks, Model 5850E series).

The protocol for obtaining in situ Raman spectra under oxidizing (O_2/Ar) and reducing (H_2/Ar) environments was as follows. The sample was initially heated at a rate of 15 °C/min in the in situ cell to 500 °C and held for 30−60 min under flowing 10% O_2/Ar (Airgas, certified, 10.00% O_2/Ar balance). Samples that are known to exhibit fluorescence were pretreated in a separate programmable furnace (Thermolyne, Model 48000) at 500 °C for 2 h under ambient air prior to the experiment. For the acquisition of the Raman spectra, only the laser angles parallel to the incident beam were allowed to hit the catalyst sample, where the accumulation was collected at 20 s/scan for 20 scans with a 200 micrometer size hole. The Raman spectra were taken at 500 °C and also at room temperature after dehydration under the oxidizing conditions. For the reduction studies, the catalyst samples were initially calcined under the same oxidizing conditions at 500 °C followed by purging of the cell with Ar (Airgas, UHP) to remove gas-phase molecular O_2. Reduction of the supported metal oxide species or silica support was not observed under the Ar environment. The catalyst temperature was adjusted to an appropriate set point before accurately introducing 1−10% H_2/Ar (Messer Gas, certified, 10.5% H_2/Ar balance). Time-resolved spectra were recorded at regular intervals to monitor the dynamic changes of the surface metal oxide species. During such reducing experiments that darken the sample, the Raman vibrations from the bulk of the SiO_2 support were used as internal standards for signal intensity.

2.3. In Situ IR Spectroscopy. The IR spectra were obtained with an FTIR spectrometer (SensIR) attached to the LabRam system (Jobin Yvon). The FTIR spectrometer was mounted on top of the LabRam HR Raman spectrometer allowing for the same spot measurement of the sample as the Raman. An all-reflecting objective (Cassegrain/Schwarzschild type) was used for the acquisition of the signal in single-beam mode, which allowed for displaying transmittance IR spectra. Mid-IR (4000−400 cm^{-1}) spectra were recorded by an MCT detector at a spectral resolution of 4 cm^{-1} using 1000 signal-averaged scans. The Linkam THMS 600 cell, housing the sample (∼5−10 mg of loose powder), was equipped with a CaF window and cooling water through the cell body. The sample temperature was controlled by the Linkam TMS94 temperature controller and calibrated externally with a secondary thermocouple (K type: Ni−Cr/Ni−Al, accuracy of 2.2 °C from −200 to 1250 °C). The true bed temperature (Y) versus controller output temperature (X) is corrected and linearly follows $Y = 0.67X$. The same gas flowrates and temperature conditions as the Linkam TS1500 for the Raman were used except the temperature range, here being 450−600 °C. The procedure protocols for sample pretreatment and gaseous environment followed the Raman experiment.

The IR spectra in Supporting Information were obtained with a BioRad FTS-40A FTIR spectrometer equipped with a DTGS detector (resolution of 2 cm^{-1}) and Perkin-Elmer 1650 FTIR spectrometer, detailed elsewhere.[49]

2.4. D_2O Exchange. The isotopic exchange of deuterium was accomplished with D_2O (Isotec, Inc., deuterium oxide "100%", 99.96 atom % D) at elevated temperatures in the in situ cell. The D_2O was directly fed into the heated inlet gas line by a liquid syringe (Hamilton, model 1005 LTN, 5.0 mL), and the gas lines were kept at a constant temperature of ∼150 °C. The flow of the deuterated water was adjusted to be 0.5−3 mol % of the total gas flowrate (∼30−50 sccm) or 0.2−1.4 μL/min, respectively, controlled by a syringe pump (Harvard Apparatus PHD 2000 Infusion, Cat. No. 70−2100). Minor adjustments were made depending on the rate of isotopic exchange per catalyst, which was monitored with online Raman spectroscopy.

2.5. In Situ UV−Vis Diffuse Reflectance Spectroscopy (DRS). The UV−vis DRS measurements were obtained with a Varian Cary 5E UV−vis-NIR spectrophotometer employing the integration sphere diffuse reflectance attachment (Harrick Praying Mantis Attachment, DRA-2). The catalyst samples were loaded as loose powder (∼20 mg) into an in situ cell (Harrick, HVC-DR2), and the spectra were collected from 200 to 800 nm. The reflectance of the SiO_2 support was used as the standard baseline. The UV−vis spectra of the metal oxide reference compounds were generally obtained under ambient conditions since adsorbed moisture does not affect their bulk structures. The supported catalyst samples, however, are sensitive to adsorbed moisture and were initially dehydrated at 400 °C from a 10 °C/min temperature ramp. The catalyst temperature was accurately controlled by a temperature program controller (Harrick Scientific, Watlow Series 965 controller) with a J-type (Iron and Constantan copper−nickel lead wires, accuracy of 2.2 °C from 0 to 750 °C) thermocouple. The catalyst samples were then held for 1 h to fully dehydrate them under flowing 10% O_2/He (Airgas, certified, 9.735% O_2/He balance) at 30 sccm. The Kubelka-Monk function, $F(R_\infty)$, was extracted from the UV−vis DRS absorbance, and the edge energy (Eg) for allowed transitions was determined by finding the intercept of the straight line from the low-energy rise of the $[F(R_\infty)h\upsilon]^{1/n}$, where $n = 0.5$ for the direct allowed transition ion, versus $h\upsilon$, the incident photon energy.[50] An example of the Eg calculation is graphically displayed in Figure S1 of Supporting Information.

3. Results

3.1. In Situ Raman and IR Spectra of the Dehydrated SiO_2 Support. The in situ Raman spectrum of the dehydrated SiO_2 support is shown in Figure 1A (top) and contains three silica network bands at ∼1065, ∼800, and 410−450 cm^{-1}, which have been assigned to the transverse-optical (TO) asymmetric stretch, Si−O−Si symmetrical stretching, and network bending modes, respectively.[51−54] A weak band at 1200 cm^{-1} is also observed, typically assigned to the longitudinal-optical (LO) silica network, but will not be discussed in greater detail since it is just beyond the M−O vibrational region that is the focus of the study. The vibrational bands at 605 and 487 cm^{-1} have been assigned to the D2 and D1 defect modes attributed to tri- and tetracyclosiloxane rings, respectively.[52,55,56] The 970 cm^{-1} Raman band arises from the Si−OH stretching mode of the surface hydroxyls.[53] The 970 cm^{-1} hydroxyl vibration is also observed in the IR spectra as shown in Figure 1A (bottom). In the

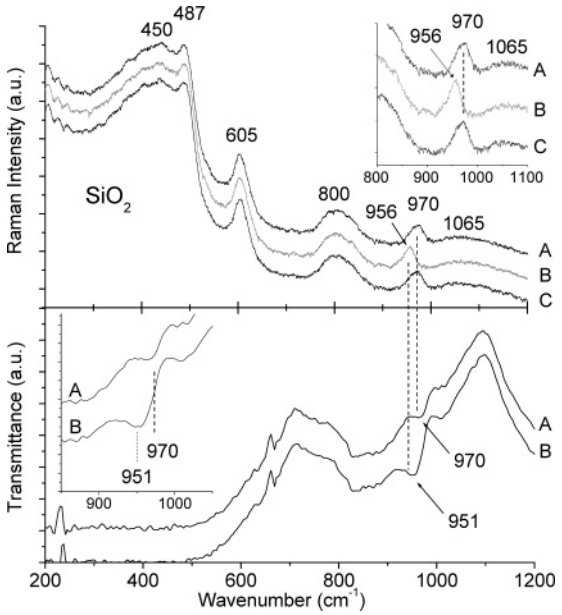

Figure 1. In situ Raman spectra of SiO_2 (top) and in situ IR spectroscopy (bottom) at 500 °C under sequential (A) oxidizing conditions, (B) D_2O, and (C) H_2O environments. Band assignments: 970 cm^{-1} [υ_s(Si−OH)]; 951−956 cm^{-1} [υ_s(Si−OD)]; remaining bands related to SiO_2 lattice.

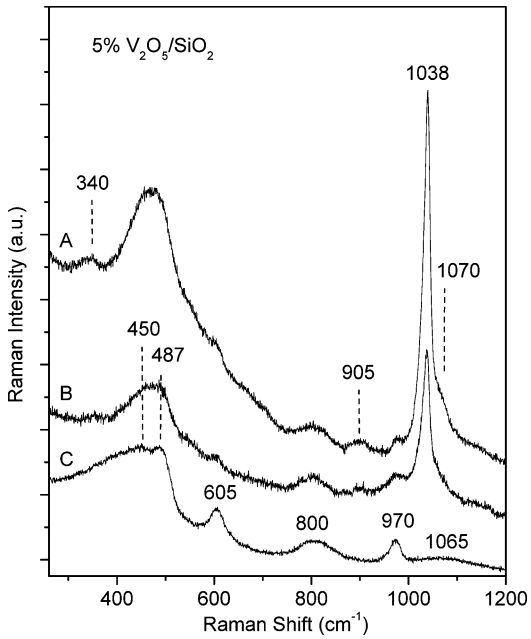

Figure 2. In situ Raman spectra of supported 5% V_2O_5/SiO_2 (532 nm) during (A) oxidizing conditions at 450 °C and (B) hydrogen reducing conditions using 5%H_2/Ar at 600 °C. The sharp band at 1038 cm^{-1} is assigned to the υ_s(V═O) species. The dehydrated SiO_2 support is shown for reference in (C). Band assignments: 1038 cm^{-1} [υ_s(V═O)]; 905 cm^{-1} [υ_s(V−O−Si)]; 340 cm^{-1} [δ(V−O)].

presence of deuterated water, both the Raman and the IR band at 970 cm^{-1} shifts to ∼950 cm^{-1}, which is attributed to the exchange of Si−(OH) to Si−(OD) (see Figure 1B). The Raman and IR spectra insets more clearly exhibit the Si−(OH) and Si−(OD) exchanged species. This is the first time that combined in situ Raman and in situ IR spectra have been employed to monitor the reversible isotopic exchange of the Si−(OH) to Si−(OD) functionalities in the 950−970 cm^{-1} region. In addition, the strong IR hydroxyl band at ∼3740 cm^{-1} (O−H stretching vibration) shifts to ∼2755 cm^{-1} (O−D stretching), not shown for brevity, which is consistent with published literature values.[57] No other vibrations assigned to the silica network are found to shift during the H_2O-D_2O exchanges, and thus, all of the additional vibrational bands originate from H-free Si−O vibrations. Subsequent injection of H_2O vapor under the same experimental conditions was also performed with SiO_2 and further confirmed the above Raman and IR spectral assignments. The relatively weak and broad Raman bands of the amorphous SiO_2 support also facilitate the detection of Raman bands from the supported metal oxide phases dispersed on the silica support.[3,28,58]

3.2. In Situ Raman Spectroscopy of Dehydrated Silica-Supported Metal Oxides. *3.2.1. Supported V_2O_5/SiO_2.* The Raman spectrum of the dehydrated supported 5% V_2O_5/SiO_2 catalyst under oxidizing conditions is shown in Figure 2A and exhibits a sharp and intense vibration at 1038 cm^{-1} that has been assigned to the terminal ν_s(V═O) stretch of isolated surface VO_4 species.[28,36,59−64] The position of the V═O vibration is in agreement with the 1034 cm^{-1} vibration of the monoxo V═O structure in the $H_3SiMo_{11}VO_{40}$ Keggin (see Table 1). The assignment of the terminal monoxo V═O vibration is also consistent with recent DFT calculations for a simple gas-phase monomer structure, O═V$(OCH_3)_3$, and monomeric polyhedral oligomeric silsesquioxane of both the cubic (O═V$Si_7O_{12}H_7$) and the hexagonal prism structures present in faujasite zeolites, calculated at ∼1038−1047 cm^{-1}.[29,30,65] In addition to the strong terminal V═O vibration at 1038 cm^{-1}, weaker bands are also present at 340 and 905 cm^{-1}, assigned to the bending (δ) V−O and stretching V−O−Si modes, respectively. The weak shoulder band at 1070 cm^{-1} is characteristic of the silica network TO mode and Si$(-O^-)_2$ and Si−O^- functionalities assigned to perturbed silica vibrations that are also indicative of the formation of V−O−Si bonds.[36] The IR spectra reveals a weak band at ∼925 cm^{-1} which likely coincides with the bridging V−O−Si support bonds (see Supporting Information, Figure S2); however, the V═O vibration at 1038 cm^{-1} is overshadowed by the strong IR absorbance of the SiO_2 support. These bridging V−O−Si support linkages calculated via DFT for both the simple monomer structure and the silsesquioxane models are estimated at 870−940 cm^{-1}.[29,65] This vibration is also present for vanadia silica xerogels in the 908−930 cm^{-1} region that has also been assigned to the bridging V−O−Si vibration.[47] The corresponding in-phase V−O stretch mode of the bridging V−O−Si bond is expected to occur at ∼1000−1030 cm^{-1}; however, this weak band is most likely overshadowed by the intense V═O stretching and Si−OH bands in this region.[30] In the 3000−4000 cm^{-1} region, a sharp Raman band at ∼3736 cm^{-1} is assigned to the isolated hydroxyl vibration (Si−O−H stretch)[57] (see Supporting Information, Figures S3) and coincides with the ∼3740 cm^{-1} band in the IR spectrum (see Supporting Information, Figures S4). The intensity of this O−H vibration for pure silica with a fully oxidized surface is approximately the same as the Si−O−Si symmetrical stretch at ∼800 cm^{-1} and the Si−(OH) band at 970 cm^{-1} and decreases upon titration of the Si−OH bonds with increasing coverage of the surface vanadia species.

The surface VO_4 species were found to be sluggish toward reduction in H_2/Ar at the elevated temperatures employed. Nevertheless, the partial reduction of the 1038, 905, and 340 cm^{-1} Raman bands at 600 °C confirm the assigned V═O, V−O−Si, and V−O vibrations to V−O vibrations (see Figure 2B).[59] Comparison of the Raman spectra for the reduced supported V_2O_5/SiO_2 catalyst sample with that of the SiO_2 support (see Figure 2C) indicated by the decrease of the 970 and 605 cm^{-1} bands upon deposition of surface vanadia indicates the preferential anchoring of the surface vanadia

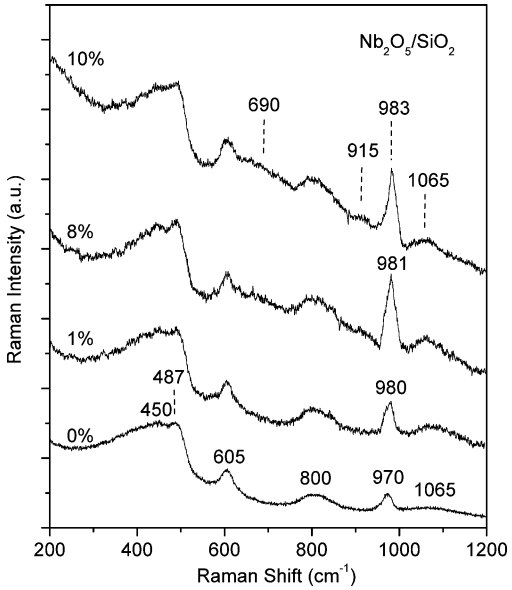

Figure 3. In situ Raman spectra of dehydrated supported Nb_2O_5/SiO_2 (532 nm) as a function of niobia loading under oxidizing conditions at 500 °C. Band assignments: 980−983 cm^{-1} [ν_s(Nb═O)]; 915 cm^{-1} [ν_s-(Nb−O−Si)]; 690 cm^{-1} (Nb_2O_5 NPs).

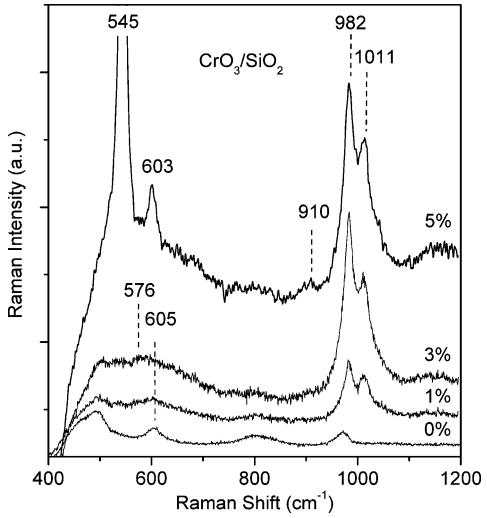

Figure 4. In situ Raman spectra of dehydrated supported CrO_3/SiO_2 (442 nm) as a function of chromia loading under oxidizing conditions at 500 °C. Band assignments: 982 cm^{-1} [ν_s(Cr(═O)$_2$)]; 1011 cm^{-1} [ν_s(Cr═O)]; 910 cm^{-1} [ν_s(Cr−O−Si)]; 576 cm^{-1} [ν_s(Cr−O−Cr)]; 545 and 603 cm^{-1} (Cr_2O_3 NPs).

species on the isolated SiO_2 support surface hydroxyls and the three-membered siloxane ring groups, respectively. The slight reduction in intensity and change in features in the 400−500 cm^{-1} region upon reduction suggest that some V−O vibrations may also exist in this region, and consequently, normalization of the reduced spectrum was performed with reference to the SiO_2 800 cm^{-1} band. Deuterated water experiments result in a shift of the 970 cm^{-1} band to ∼955 cm^{-1} (see Supporting Information, Figure S5) due to the exchange of Si−(OH) into Si−(OD) as seen with the pure silica, which is similar to Figure 1. The main surface vanadia bands at 1038, 905, and 340 cm^{-1} as well as the SiO_2 support vibrations at 605, 800, and 1070 cm^{-1} do not shift during the H_2O-D_2O exchange environment establishing that none of these vibrations arise from either V−OH or Si−OH functionalities.

3.2.2. Supported Nb_2O_5/SiO_2. The Raman spectra of the dehydrated supported Nb_2O_5/SiO_2 catalysts under oxidizing conditions are presented in Figure 3 and exhibit a sharp ν_s(Nb═O) band at 980−983 cm^{-1} that increases with surface niobia coverage.[39,66] This vibration has been assigned to the monoxo Nb═O vibration of surface NbO_4 species[39,67,68] and is consistent with monoxo Nb═O vibrations in bulk niobium oxide reference compounds (see Table 1).[19] A weak and broad band at 915 cm^{-1} also increases with niobia loading and is representative of the bridging Nb−O−Si vibration; however, this band is obstructed by the strong absorbance of the SiO_2 vibration in the IR spectra (see Supporting Information, Figure S6). In addition, a weak and broad Raman band is present for all Nb loadings at ∼1065 cm^{-1} assigned to the TO of the silica network. The much weaker intensity of the Raman bands for the surface NbO_4 species compared with the surface VO_4 makes the detection of bending modes in the 200−400 cm^{-1} region very difficult to observe against the stronger silica background. For the 10% Nb_2O_5/SiO_2 catalysts, a weak and broad band also appears at ∼690 cm^{-1} and is assigned to the formation of crystalline Nb_2O_5 nanoparticles (NPs).[19,39,67] Therefore, the maximum surface niobia dispersion on the SiO_2 support without the presence of crystalline Nb_2O_5 NPs is achieved for the 8% Nb_2O_5/SiO_2 (1.1 Nb atoms/nm^2) catalyst sample in this study.

The surface NbO_4 species are found to be very stable toward reduction in the 5% H_2/Ar gaseous mixture at 500−600 °C. Reduction at higher temperatures is expected to alter the structures of the initial surface niobia species as well as the silica support, which would make such information tenuous at best. Under D_2O environments, the ∼980 and 915 cm^{-1} bands of the surface niobia species and silica vibrations at 487, 605, 800, and 1065 cm^{-1} do not shift (see Supporting Information, Figure S7). The absence of any vibrational shifts for the Raman bands during the H_2O-D_2O exchange studies establishes that none of these vibrations are related to either Nb−OH or Si−OH functionalities, which indicates that the silica surface hydroxyl were extensively titrated by the surface niobia species.

3.2.3. Supported Ta_2O_5/SiO_2. The weak Raman scattering of the dehydrated surface TaO*x* species does not give rise to any distinct vibrations against the stronger SiO_2 support vibrations, and consequently, the Raman spectra are not shown for brevity.[40,69] In addition, crystalline Ta_2O_5 NPs are not detected for 1−10% Ta_2O_5/SiO_2 catalysts, which would appear at 105, 253, and ∼630 cm^{-1}.[68,70] The maximum surface tantala dispersion on the SiO_2 support without the presence of crystalline Ta_2O_5 NPs is achieved for the 10% Ta_2O_5/SiO_2 (∼0.8 Ta atoms/nm^2) catalyst in this study, which is consistent with previously reported XPS studies.[40] Reduction and D_2O exchange studies were not undertaken because of the stability of the surface TaO*x* species toward reduction and the absence of detectable Raman vibrations of the surface TaO*x* species.

3.2.4. Supported CrO_3/SiO_2. The in situ Raman spectra of the dehydrated supported 1−5% CrO_3/SiO_2 catalysts under oxidizing conditions were collected with 442 nm excitation to avoid sample fluorescence at 532 nm[42,71] and to also take advantage of the known resonance enhancement of the surface CrO*x* species at this excitation frequency.[41,72] The Raman spectra of the dehydrated supported CrO_3/SiO_2 catalysts are presented in Figure 4 and exhibit two major bands at 982 and 1011 cm^{-1}. These bands have been assigned to Cr═O vibrations and monotonically increase with surface chromia coverage. The 5% CrO_3/SiO_2 catalyst spectrum also contains a weak band from the bridging Cr−O−Si vibration at ∼910 cm^{-1}, which is more clearly observed in the complementary IR spectra (see Supporting Information, Figure S8). These Raman bands are also

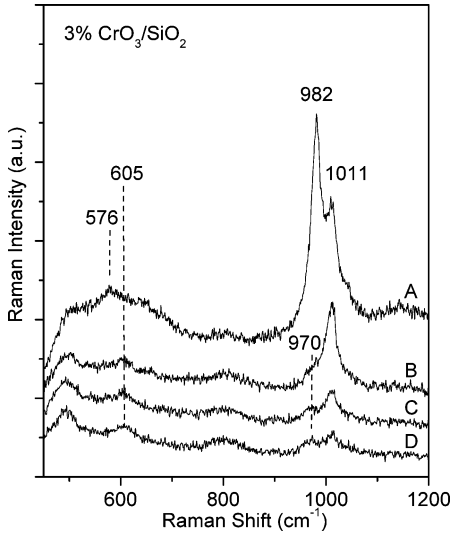

Figure 5. In situ Raman spectra of dehydrated 3% CrO_3/SiO_2 (442 nm) at 500 °C under (A) oxidizing conditions and exposed to 5% hydrogen reduction environments taken after (B) ~5 min, (C) ~25 min, and (D) ~90 min. Band assignments: 982 cm^{-1} [υ_s(Cr(═O)$_2$)]; 1011 cm^{-1} [υ_s(Cr═O)]; 576 cm^{-1} [υ_s(Cr—O—Cr)].

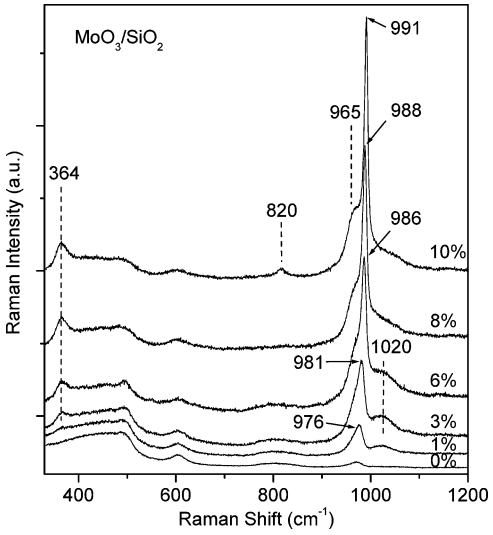

Figure 6. In situ Raman spectra of dehydrated MoO_3/SiO_2 (325 nm) under oxidizing conditions at 500 °C. Band assignments: 976—991 cm^{-1} [υ_s(Mo(═O)$_2$)]; 965 cm^{-1} [υ_{as}(Mo(═O)$_2$)]; 1020 cm^{-1} [υ_s(Mo═O)]; 364 cm^{-1} [δ(O—Mo—O)]; 820 cm^{-1} [MoO_3 NP].

accompanied by a weak band at 576 cm^{-1} that is typical of Cr—O—Cr vibrations for the 1—3% CrO_3/SiO_2 catalysts.[41] The associated O—Cr—O bending vibration in the ~300—400 cm^{-1} range could not be collected because of the 442 nm notch filter cutoff at ~450 nm. This region, however, could be accessed with 325 nm excitation that reveals a Raman band from the O—Cr—O bending modes at ~396 cm^{-1} (not shown for brevity). The presence of crystalline Cr_2O_3 NPs in the supported 5% CrO_3/SiO_2 catalyst is also indicated by its strong characteristic vibrations at 545 and 603 cm^{-1}.[42] Therefore, the highest surface chromia dispersion achieved without the presence of crystalline Cr_2O_3 NPs corresponds to ~3—4% CrO_3/SiO_2 (~0.6—0.8 Cr atoms/nm^2) for the present set of supported CrO_3/SiO_2 catalysts.

In situ Raman spectroscopy of the supported 3% CrO_3/SiO_2 catalyst under H_2-reducing environments reveals additional insights that could not be obtained under the oxidizing conditions. Upon reduction, the Raman bands at 982 and 1011 cm^{-1} from the terminal Cr═O functionality decrease in intensity because of reduction of the surface CrO*x* species (see Figure 5). From time-resolved Raman spectroscopy, it is further seen that the 982 and 1011 cm^{-1} bands reduce in intensity at different rates with the sharp band at 982 cm^{-1} disappearing faster than the 1011 cm^{-1} band (see Figure 5B). This difference suggests that these two Raman bands do not originate from the same surface chromia species. Furthermore, the possibility that the surface CrO*x* species at 982 cm^{-1} preferentially reduces to the surface CrO*x* species at 1011 cm^{-1} is not feasible since both surface species are fully oxidized as surface Cr^{+6} and the location of Cr═O vibration of a partially reduced Cr^{+4} species would not be expected to vibrate at the same position for Cr^{+4}═O and Cr^{+6}═O species. The band at 982 cm^{-1} is consistent with the dioxo O═Cr═O functionality of the $(Ph_3SiO)_2CrO_2$ reference compound in Table 1, and the band at 1011 cm^{-1} is characteristic of a monoxo Cr═O surface CrO*x* species (see Table 1). At longer H_2 reduction times, the band at 1011 cm^{-1} is almost completely removed (see Figure 5D), and only the spectrum of the SiO_2 support remains. Note that the weak vibration at 970 cm^{-1} band from the vibration of the remaining untitrated surface Si—OH sites is also detectable. The weak and broad Raman band at ~576 cm^{-1} is also removed with the reduction treatment. The elimination of the 1011, 982, and 576 cm^{-1} Raman bands upon reduction confirms that these bands are associated with Cr—O vibrations.

3.2.5. Supported MoO_3/SiO_2. The Raman spectra of the dehydrated supported 1—8% MoO_3/SiO_2 catalysts under oxidizing conditions give rise to the strongest surface metal oxide signals among the SiO_2 supported transition metal oxide catalysts examined. The major Raman band appears at 976—991 cm^{-1} and slightly shifts with surface molybdena coverage on the SiO_2 support as shown in Figure 6. The progressive shift of this surface molybdena band toward higher wavenumbers is most probably related to lateral interactions among adjacent surface MoO*x* species (increased distortion with surface coverage or the decreased surface concentration of SiOH sites with increasing surface molybdena loading). The monoxo $H_3SiMo_{12}O_{40}$ Keggin structure gives rise to a Raman band at 1006 cm^{-1}, and DFT calculations predict that monoxo (Si—O)$_4$Mo═O and dioxo (Si—O)$_2$Mo(═O)$_2$ should vibrate at 1014—1017 and 995 (υ_s)/977 (υ_{as}) cm^{-1}, respectively.[32] Consequently, the surface molybdena vibrations at 976—991 cm^{-1} correspond to dioxo surface O═Mo═O species in the supported MoO_3/SiO_2 catalyst samples (see Table 1). The weak and broad Raman band at ~965—975 cm^{-1}, on the left shoulder of the main Raman band, is the corresponding asymmetric stretch of the dioxo O═Mo═O structure.[23,32] The O—Mo—O bending mode of the surface molybdena species is also observed at 364 cm^{-1}. Another broad and weak band at ~1020 cm^{-1} is observed to increase until ~6% MoO_3/SiO_2 and coincides to the vibration expected for monoxo M═O structures at 1006—1017 cm^{-1} (see Table 1). This band is tentatively assigned to a second dehydrated surface molybdena species. The surface molybdena species Raman bands at 364, ~965, 976—991, and 1020 cm^{-1} do not shift during the H_2O—D_2O exchange, which is consistent with the absence of a Mo—OH functionality (see Supporting Information, Figure S9). The expected weak bridging Mo—O—Si band is not readily observed in the ~900—930 cm^{-1} region of the Raman and IR spectra (see Supporting Information, Figure S10) and could be overshadowed by the intense Raman bands of the surface molybdena species. Similarly, the TO silica network band at 1065 cm^{-1} is probably overshadowed by the 1020 cm^{-1} band. A small amount of crystalline MoO_3 NPs is also present in the supported 10% MoO_3/SiO_2 catalyst since the characteristic MoO_3 vibration at ~820 cm^{-1} is present in

TABLE 2: Band Maxima and Eg Values for Dehydrated Supported MO*x*/SiO_2 Catalysts, Where M Represents the Group 5, 6, and 7 Transition Metal Oxides, as a Function of Loading

catalyst	V_2O_5/SiO_2		Nb_2O_5/SiO_2		Ta_2O_5/SiO_2		CrO_3/SiO_2		MoO_3/SiO_2		WO_3/SiO_2		Re_2O_7/SiO_2	
loading (wt %)	band (nm)	Eg (eV)	band (nm)	Eg (eV)	band (nm)	Eg (eV)	bands (nm)	Eg (eV)	bands (nm)	Eg (eV)	bands (nm)	Eg (eV)	band (nm)	Eg(eV)
0.5%							251, 348, 460	2.48						
1%	273	3.60	250	4.29	220	5.08	246, 338, 460	2.45	234, 270	4.18	228, 261	4.18	238	4.75
3%							246, 337, 460	2.41	237, 274	4.13	231, 265	4.12	240	4.67
5%	287	3.47	250	4.28	222	5.13	247, 340, 458, 602	1.81[a]	239, 276	4.07	235, 270	4.03	241	4.67
6%									240, 277	4.04	235, 270	4.00		
8%	289	3.45	250	4.26	223	5.20			240, 280	3.97	235, 270, ~400 (sh.)	3.82[a]		
10%	296	3.43	252	4.20	223	5.16			240, 281, ~400 (sh.)	3.91[a]				

[a] Indicates presence of crystallite species observed by Raman spectroscopy.

the Raman spectrum of this catalyst sample. Therefore, the maximum molybdena loading achieved with only molecularly dispersed surface MO*x* species on SiO_2 with the present catalysts is obtained with the supported 8% MoO_3/SiO_2 (1.0 Mo atoms/nm^2) catalyst.

The in situ Raman spectral changes of the supported 3% MoO_3/SiO_2 catalyst during hydrogen reduction are presented in Figure 7. The extent of reduction of the surface MO*x* species, represented by the Raman band at 981 cm^{-1}, is about 1/2 and 1/4 of the fully oxidized sample under 2% and 5% H_2/He (see Figure 7C,D), respectively. Higher H_2 concentrations or temperatures were not examined because such reducing conditions can damage the in situ cell.[73] The decrease in intensity of the Raman bands at 364, ~965, 981, and 1020 cm^{-1} during the H_2 reduction treatments confirms these assignments as originating from Mo−O vibrations. The SiO_2 vibrations, however, are not affected by the H_2 reduction treatments. Oxidation of the partially reduced supported MoO_3/SiO_2 catalysts restores all of the surface MO*x* vibrations (see Figure 7B).

3.2.6. Supported WO_3/SiO_2. The Raman spectra of the dehydrated supported WO_3/SiO_2 catalysts under oxidizing conditions give rise to weak surface WO*x* vibrational bands as shown in Figure 8. The combination of weak surface WO*x* vibrations and sample fluorescence prevented the collection of Raman spectra of the supported 1−4% WO_3/SiO_2 catalysts. For the 5 and 6% WO_3/SiO_2 catalysts, however, two terminal W═O Raman bands are present at ~985 and 1014 cm^{-1}. The presence of two distinct surface WO*x* species is supported by the variation of the relative intensity of these two Raman bands with temperature (not shown for brevity). The intensity ratio of the Raman bands at 1014 and 985 cm^{-1} are ~2:1, 1:1, and 1:4 at 200, 400, and 800 °C, respectively. The sum of the two peak areas remains constant throughout the wide temperature range suggesting comparable Raman cross sections for the two surface tungsta species. Monoxo W═O structures possess W═O vibrations at ~1020−1022 cm^{-1} (see Table 1), and dioxo O═W═O structures are expected to vibrate at 998(υ_s)/972(υ_{as}) cm^{-1} (see Table 1). By comparison, the 985 cm^{-1} band is assigned to the surface dioxo O═W═O species, and the 1014 cm^{-1} band is assigned to the surface monoxo W═O species. The Raman shoulder at ~968 cm^{-1} is assigned to the asymmetric vibration of the dioxo O═W═O functionality (see Table 1). A weak band at 346 cm^{-1} is also present and is assigned to the O−W−O bending mode of surface WO*x*. The bridging W−O−Si band is likely the weak and broad band at ~900 cm^{-1} that is subtly observed to have a noticeably different slope than the silica support, which likely corresponds to the weak shoulder at 923 cm^{-1} from the IR spectra (see Supporting Information, Figure S11). The weak and broad TO silica network vibration at 1065 cm^{-1} slightly shifts to 1050 cm^{-1} because of its overlap with the 1014 cm^{-1} vibration. The absence of any significant vibrational shifts during the H_2O-D_2O exchange experiments further supports that the vibrations from the surface WO*x* species do not contain the W−OH functionality and also that the 968 cm^{-1} vibration is not related to the Si−OH species expecting that should shift ~950 cm^{-1} (see Supporting Information, Figure S12). The dehydrated supported 8% WO_3/SiO_2 catalyst additionally contains crystalline WO_3 NPs, which are reflected by the strong bands at ~800 and 712 cm^{-1}.[74] Thus, the highest tungsten oxide dispersion achieved in the present study without the presence of crystalline WO_3 NPs is 6% WO_3/SiO_2 (0.5 W atoms/nm^2).

The surface WO*x* species were found to be very stable to reduction environments under the 5% H_2/He gaseous mixture at 500−600 °C. Likewise, the vibrations of the silica support were not affected under hydrogen treatment conditions. Consequently, further surface reduction studies of the supported WO_3/SiO_2 catalysts were not undertaken.

3.2.7. Supported Re_2O_7/SiO_2. The Raman spectra of the dehydrated supported Re_2O_7/SiO_2 catalysts under oxidizing conditions exhibit a sharp band at 1010 cm^{-1} and are shown in Figure 9. The position of this Raman band coincides with the symmetric stretch at 1009 cm^{-1} of the trioxo Re(═O)$_3$ functionality in the gas-phase (O═)$_3$Re−O−Re(═O)$_3$ molecule (see Table 1). The corresponding asymmetric stretch for gaseous Re_2O_7 dimers vibrates at 972 cm^{-1}, which corresponds to the weaker 977 cm^{-1} band in the dehydrated supported Re_2O_7/SiO_2 spectra. The 977 cm^{-1} band from the surface ReO*x* species also overlaps with the Si−OH band at 970 cm^{-1}, which broadens the band and makes it appear more intense. The associated bending δ(O−Re−O) mode of the gaseous Re_2O_7 dimer occurs at 341 cm^{-1}, which coincides with the weak band observed at 343 cm^{-1} for the dehydrated supported Re_2O_7/SiO_2 catalysts. These surface ReO*x* bands increase in intensity with loading and are in excellent agreement with the same functionalities found in the gas-phase trioxo Re_2O_7 structure, with the exception of bridging Re−O−Re vibration that is only present in the gaseous Re_2O_7 dimer. Thus, the local structure of the dehydrated surface ReO*x* species is a surface trioxo Re(═O)$_3$ species. The bridging Re−O−Si band is expected to give rise to a weak band at ~900 cm^{-1} that is not readily apparent in the Raman and IR spectra (see Supporting Information, Figure S13) of the dehydrated supported catalysts. The TO silica network band of the SiO_2 support at 1065 cm^{-1} also appears as a small shoulder on the stronger Re═O vibration at 1010 cm^{-1}. During H_2O-D_2O exchange experiments, the unreacted Si−OH sites exchanged to Si−OD, which is observed by the shift of the 977 cm^{-1} band to ~968 cm^{-1}, respectively (see Supporting Infor-

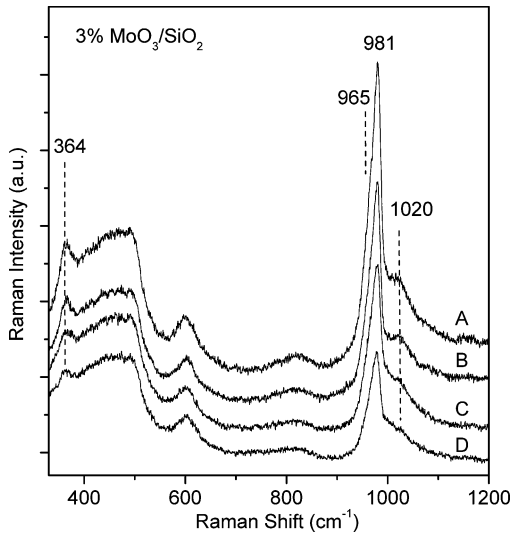

Figure 7. In situ Raman spectra of dehydrated supported 3% MoO_3/SiO_2 (325 nm) at 500 °C under (A) oxidizing, dehydrated conditions, (B) reoxidation after reduction environments, (C) 2% H_2/He, and (D) 5% H_2/He. Band assignments: 981 cm^{-1} [υ_s(Mo(═O)$_2$)]; 965 cm^{-1} [υ_{as}(Mo(═O)$_2$)], 1020 cm^{-1} [υ_s(Mo═O)]; 364 cm^{-1} [δ(O─Mo─O)].

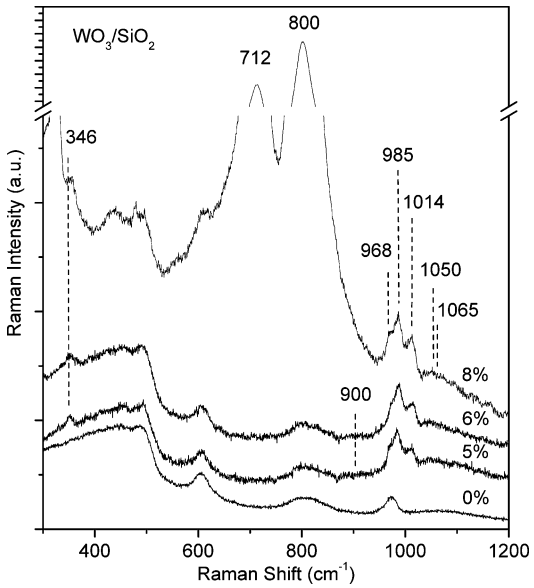

Figure 8. In situ Raman spectra of dehydrated supported WO_3/SiO_2 (532 nm) under oxidizing conditions at 500 °C. Band assignments: 985 cm^{-1} [υ_s(W(═O)$_2$)]; 968 cm^{-1} [υ_{as}(W(═O)$_2$)]; 1014 cm^{-1} [υ_s(W═O)]; 900 cm^{-1} [υ_s(W─O─Si)]; 346 cm^{-1} [δ(O─W─O)]; 800 and 712 cm^{-1} (WO_3 NPs).

mation, Figure S14). The strong Raman bands at 343 and 1010 cm^{-1} from the surface trioxo Re(═O)$_3$ species, however, do not shift during H_2O-D_2O exchange and reflect that these vibrations are not associated with Re─OH vibrations. The SiO_2 bands, particularly the TO vibration of the silica network at ~1065 cm^{-1}, are also not perturbed by the H_2O-D_2O exchange. The maximum attainable surface rhenia coverage for the Re_2O_7/SiO_2 catalysts is always significantly less than monolayer coverage because the surface rhenium oxide species readily recombine to form volatile gaseous Re_2O_7 dimers.[45] Consequently, crystalline Re_2O_7 is never present for supported Re_2O_7 catalysts.[23] The highest loading silica-supported rhenia sample synthesized in this study is the supported 5% Re_2O_7/SiO_2 catalyst (0.4 Re atoms/nm^2).

The dehydrated surface ReO_4 species on SiO_2 readily reduce upon exposure to H_2/Ar at 450 °C as shown in Figure 10. The complete removal of the Raman bands from supported Re_2O_7/SiO_2 at 1010, 977, and 343 cm^{-1} confirm that these vibrations are associated with the surface trioxo Re(═O)$_3$ species (see Figure 10C). These three Raman bands are readily restored by oxidation of the reduced catalysts (see Figure 10B). Note that the Raman spectrum of the reduced supported Re_2O_7/SiO_2 catalyst looks exactly like the Raman spectrum of the dehydrated SiO_2 support (see Figure 10D) and demonstrates that the SiO_2 support is not reduced by the reduction treatments. The residual presence of the Si─OH Raman band at 970 cm^{-1} is consistent with the above finding that the low surface rhenia coverage on the SiO_2 support leaves many unreacted Si─OH sites on the SiO_2 support.

3.3. In Situ UV−Vis DRS of Dehydrated Silica-Supported Metal Oxides. *3.3.1. Supported V_2O_5/SiO_2.* The in situ UV−vis DRS of the dehydrated supported 1−10% V_2O_5/SiO_2 catalysts are shown in Figure 11, and the corresponding Eg values are tabulated in Table 2. The LMCT band maximum shifts from 273 to 296 nm, and the corresponding Eg values shift from ~3.6 to ~3.4 eV with increasing surface vanadia coverage. The single LMCT transition and narrow range of Eg values are consistent with the values of isolated vanadium oxide reference compounds, such as Na_3VO_4 in Table 3, and are quite different than those of the polymeric VO_4 or bulk-like reference

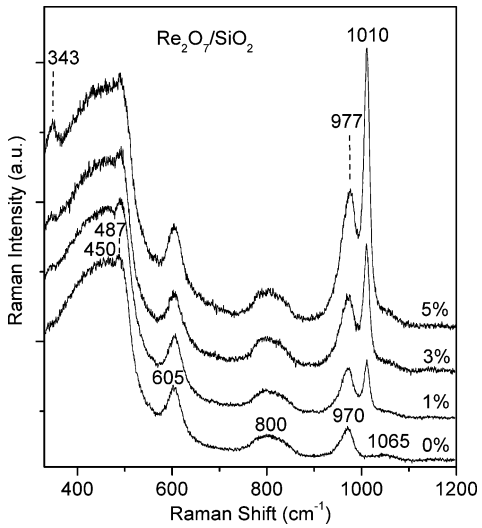

Figure 9. In situ Raman spectra of dehydrated Re_2O_7/SiO_2 (325 nm) under oxidizing conditions at 450 °C. Band assignments: 1010 cm^{-1} [υ_s(Re(═O)$_3$)]; 977 cm^{-1} [υ_{as}(Re(═O)$_3$)]; 343 cm^{-1} [δ(O─Re─O)].

compounds (see Supporting Information, Figure S15). Thus, the dehydrated surface vanadia species on SiO_2 are present as isolated VO_4 species.

3.3.2. Supported Nb_2O_5/SiO_2. The in situ UV−vis DRS of the dehydrated supported 1−10% Nb_2O_5/SiO_2 catalysts are also shown in Figure 11 and give rise to a single LMCT band at ~250 nm with an Eg value of 4.3−4.2 eV (see Table 2). The LMCT band maximum does not shift to higher wavelengths, and the Eg value is relatively constant indicating that the same surface NbO*x* species are present at all coverage. The trace amount of crystalline Nb_2O_5 NPs detected with Raman for the dehydrated 10% Nb_2O_5/SiO_2 catalyst has only a minimal effect on the overall UV−vis DRS Eg value for this catalyst sample. Comparison with the dehydrated supported Nb−MCM41 (see Table 3), which contains isolated surface NbO_4 species, suggests

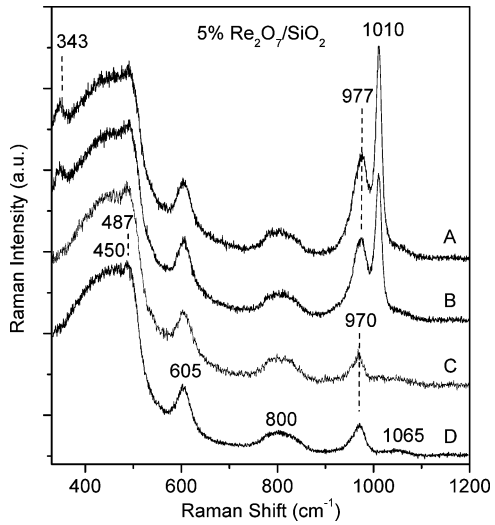

Figure 10. In situ Raman spectra of 5% Re_2O_7/SiO_2 (325 nm) at 450 °C under (A) oxidizing conditions, (B) reoxidation after reduction with 2% H_2/Ar, and (C) reduction with 2% H_2/Ar. The SiO_2 support reference spectrum is shown in (D). Band assignments: 1010 cm^{-1} [ν_s(Re(═O)$_3$)]; 977 cm^{-1} [ν_{as}(Re(═O)$_3$)]; 343 cm^{-1} [δ(O−Re−O)].

that the dehydrated surface NbO*x* species on SiO_2 also consist of isolated surface NbO_4 species.[39]

3.3.3. Supported Ta_2O_5/SiO_2. The in situ UV−vis DRS of the dehydrated supported 1−10% Ta_2O_5/SiO_2 catalysts are shown in Figure 11 and reveal a single, narrow LMCT band at ∼220 nm with an Eg value of 5.0−5.2 eV (see Table 2). Similar to dehydrated silica supported VO*x* and NbO*x* catalysts, the same surface TaO*x* species are present at all coverage since the LMCT band maximum does not shift to higher wavelengths, and the Eg value remains constant. The Eg value and LMCT band maximum positions closely resemble those of the low coverage dehydrated Ta/xerogels that contain isolated TaO_4 species (see Table 3). Therefore, the dehydrated surface tantala species on SiO_2 are also concluded to possess TaO_4 coordination.[40,75] The absence of the ∼265 nm LMCT band of crystalline Ta_2O_5 confirms the sole presence of dehydrated isolated surface TaO_4 species on silica.[69]

3.3.4. Supported CrO_3/SiO_2. The in situ UV−vis DRS of the dehydrated supported 0.5−3% CrO_3/SiO_2 catalysts are presented in Figure 12 and exhibit multiple LMCT transitions at ∼250, ∼340, and ∼460 nm. The UV−vis DRS band intensity increases almost linearly, and the band maximum does not shift with increasing surface chromia coverage. The constancy of these parameters suggests that the surface CrO*x* species are similar at all loadings for the dehydrated supported CrO_3/SiO_2 catalysts below the maximum dispersion limit. From the best linear fit in the lower absorption region, the calculated Eg values are between 2.5 and 2.4 eV (see Table 2). For the 5% CrO_3/SiO_2, which contains crystalline Cr_2O_3 NPs detected by Raman spectroscopy, an additional d−d transition at ∼600−700 nm is also present similar to bulk Cr_2O_3 with a corresponding Eg value of ∼1.8 eV. Aside from this high loaded catalyst with Cr_2O_3 NPs, the UV−vis DRS band maxima for the dehydrated supported CrO_3/SiO_2 catalysts are in good agreement with those for both isolated CrO_4 monomers incorporated into mesoporous silica with wormhole structures, HMS,[72,76] and highly dispersed, isolated Cr(VI) species in a silica xerogel monolith.[47] Furthermore, the Eg values of the dehydrated supported silica system closely follow those of the isolated structures present in the bulk $MgCrO_4$, $(NH_4)_2CrO_4$, and K_2CrO_4 reference compounds (see Table 3). Thus, the dehydrated supported CrO_3/SiO_2 catalysts primarily consist of isolated CrO*x* species at low loadings.

3.3.5. Supported MoO_3/SiO_2. The in situ UV−vis DRS spectra of the dehydrated 1−8% MoO_3/SiO_2 catalysts are shown in Figure 12 and possess two LMCT transitions with band maxima at ∼230 and ∼275 nm. The corresponding UV−vis DRS Eg values from the lower absorption rise of the low-energy region are ∼4.0−4.2 eV (see Table 2). The LMCT band maxima and Eg values are invariant with surface MoO*x* coverage and suggest that the nature of the surface species is constant with molybdena loading. Comparison of these Eg values for the dehydrated supported MoO_3/SiO_2 catalysts with known MoO*x* molecular structures, for example, isolated MoO_4 sites in bulk $Al_2(MoO_4)_3$ and $MgMoO_4$ shown in Table 3, are consistent with isolated monomeric MoO*x* species. The dehydrated 10% MoO_3/SiO_2 catalyst, however, contains an additional weak transition at ∼400 nm, which lowers the Eg value to ∼3.9 eV, from the presence of a small amount of crystalline MoO_3 NPs that have readily been detected by Raman spectroscopy (see above).

3.3.6. Supported WO_3/SiO_2. The in situ UV−vis DRS of the dehydrated supported WO_3/SiO_2 catalysts were collected after calcination at 400 °C in order to maximize the surface dioxo O═W═O population since it was found to predominate at elevated temperatures. The UV−vis DRS of the dehydrated supported 1−6% WO_3/SiO_2 catalysts are shown in Figure 13 and exhibit band maxima at ∼230 and ∼265 nm with corresponding Eg values of 4.0−4.2 eV (see Table 2). Comparison with the Eg values of the known WO*x* molecular structures listed in Table 3, for example, isolated WO_4 in ZrW_2O_8, $Al_2(WO_4)_3$, and WO*x*/xerogels, suggests that dehydrated isolated surface WO*x* species are the predominant species. The dehydrated 8% WO_3/SiO_2 catalyst, which contains an additional weak transition at ∼400 nm, lowers the Eg value to ∼3.8 eV because of the minor presence of crystalline WO_3 NPs detected with Raman spectroscopy (see above).

3.3.7. Supported Re_2O_7/SiO_2. The in situ UV−vis DRS of the dehydrated supported 1−5% Re_2O_7/SiO_2 catalysts are presented in Figure 13 and give rise to a single LMCT transition at ∼240 nm with a corresponding Eg value of ∼4.7 eV (see Table 2). The UV−vis DRS band maxima and Eg values for the dehydrated supported Re_2O_7/SiO_2 catalysts are comparable to the rhenia reference compounds with isolated ReO_4 molecular structures that are given in Table 3.

4. Discussion

The in situ Raman and IR band positions and their assignments as well as the corresponding in situ UV−vis DRS edge energy values for the dehydrated surface metal oxide on SiO_2 catalyst samples are summarized in Table 4. In addition, the dehydrated molecular structures of the dominant isolated, surface MO_x species on silica of supported group 5, 6, and 7 metal oxide catalysts are depicted in Figure 14. Some of the critical issues surrounding each of the silica-supported metal oxide system are elaborated upon further below.

4.1. Molecular Structures of the Dehydrated Group 5 Surface Metal Oxides on Silica. *Supported V_2O_5/SiO_2.* The dehydrated surface VO*x* species are isolated (high Eg value from UV−vis DRS), and the location of the V═O vibration is only consistent with one terminal V═O bond (see Table 1). This assignment is further supported by only one V═O IR band in the overtone region,[60] the absence of an associated ν_{as} stretch and the presence of only two bands during $^{18}O_2-^{16}O_2$ exchange studies (V═^{16}O and V═^{18}O).[77] The isolated, monoxo surface O═V(−O−Si)$_3$ structure present for the dehydrated supported V_2O_5/SiO_2 catalyst system is fairly well-established from multiple spectroscopic characterization techniques and even DFT

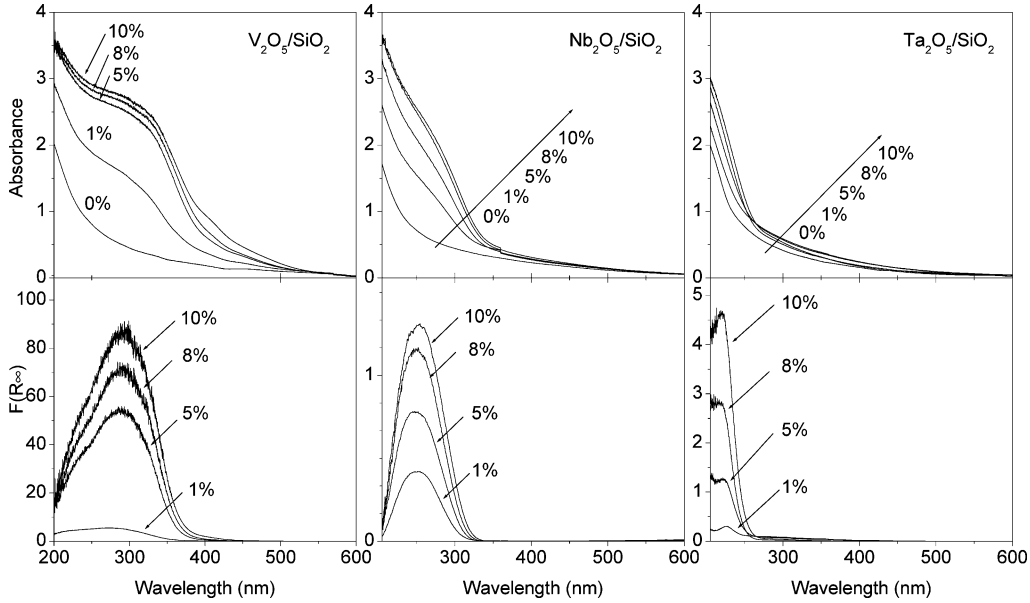

Figure 11. In situ UV−vis DRS spectra of dehydrated V_2O_5/SiO_2, Nb_2O_5/SiO_2, and Ta_2O_5/SiO_2.

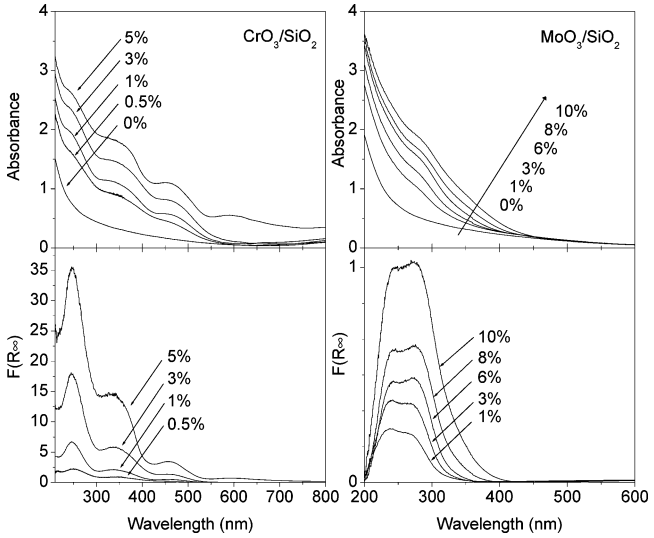

Figure 12. In situ UV−vis DRS spectra of dehydrated CrO_3/SiO_2 and MoO_3/SiO_2.

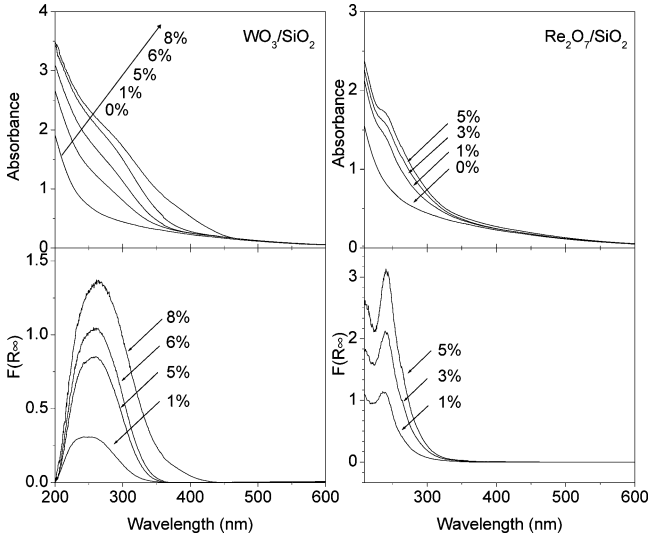

Figure 13. In situ UV−vis DRS spectra of dehydrated WO_3/SiO_2 and Re_2O_7/SiO_2.

theoretical calculations.[29,30,65] More recently, some researchers have also proposed that a V−OH functionality is also present for the dehydrated surface VO_4 species on the basis of a detected IR band at 3660 cm^{-1}.[78−82] The vibrations of the surface VO_4 species (1034, 905, and 324 cm^{-1}), however, are not perturbed by the isotopic H_2O-D_2O exchange, and only the exchange from Si−(OH) to Si−(OD) takes place (from 970 to 956 cm^{-1} and 3736 to 2755 cm^{-1}, respectively). In addition, the reported IR band at ∼3660 cm^{-1} was not detected under dehydrated conditions by both Raman and IR spectroscopy in the present investigation (see Supporting Information, Figure S4). Many researchers have only observed the 3660 cm^{-1} IR band after exposing the dehydrated supported V_2O_5/SiO_2 catalysts to moisture at low temperatures.[81,82] Only when ambient moisture was introduced to the dehydrated supported V_2O_5/SiO_2 catalyst at 300 °C in the present study did the 3660 cm^{-1} band appear (see Supporting Information, Figure S4). It appears that the IR studies that have claimed the existence of a V−OH functionality for the dehydrated surface vanadia species most probably did not have a moisture-free environment that caused partial hydration.[78−80] Furthermore, the exact location of the −OH functionality created by moisture at low temperature is presently not known since no cross-polarized $^{51}V-^{1}H$ NMR measurements have been made to determine if the 3660 cm^{-1} hydroxyl present upon partial hydration is associated with V−OH or Si−OH sites. Another structure for the surface VO*x* species has recently been proposed, the "upside down ΛO_4 structure";[83] however, more experimental and theoretical work is needed to address this hypothesis.

Supported Nb_2O_5/SiO_2. The dehydrated surface NbO*x* species are isolated (high Eg value from UV−vis DRS), and the position of the Nb═O vibration is consistent with one terminal Nb═O bond (see Table 1). As for supported O═V(−O−Si)$_3$, the detailed in situ Raman and UV−vis spectroscopic studies are representative of only one isolated surface monoxo O═Nb(−O−Si)$_3$ structure at all surface coverage below the maximum dispersion limit.[66] The absence of any Raman shifts in the surface niobia vibrations during isotopic H_2O-D_2O exchange reveals that the dehydrated surface niobia species do not contain the Nb−OH functionality. An alternative surface NbO*x* structure on SiO_2 has been proposed for the dehydrated species from EXAFS measurements. It has been proposed that two dehydrated

TABLE 3: Uv−vis DRS Eg Values for Group 5, 6, and 7 Metal Oxide Reference Compounds Recorded under Ambient Conditions unless Otherwise Indicated

metal oxide reference compound	band maxima (nm)	Eg (eV) (hydr.)	molecular structure
V compounds			
V_2O_5	236, 334, 481	2.3	polymeric VO_5 3D structure[36,108]
MgV_2O_6	250, 370	2.8	polymeric VO_6[36]
$NaVO_3$, NH_4VO_3	∼285, ∼360	3.2	polymeric VO_4[36]
$Mg_2V_2O_7$	280	3.5	dimeric VO_4[36]
$Mg_3V_2O_8$, Na_3VO_4	∼260, ∼300	3.5−3.9	isolated VO_4[36]
Nb compounds			
Nb_2O_5	282	3.4	polymeric $NbO_{6,7,8}$ 3D structure[19,39,108]
$KNbO_3$, $NaNbO_3$	278, 305, 341 (sh.)	3.4−3.5	polymeric NbO_6[19,39]
$LiNbO_3$	284	3.9	polymeric NbO_6[19,39]
Nb-MCM41	245	4.4	isolated NbO_4[39]
Ta compounds			
Ta_2O_5	271	3.8	polymeric TaO_6/TaO_7 3D structure[23,75,108]
$MgTa_2O_6$	222, 264, 300 (sh.)	4.0	distorted TaO_6[75,109]
8% Ta−MCM-41	228, 264 (sh.)	4.6[a]	isolated TaO_4[75]
0.25% Ta−MCM-41	228	4.8[a]	isolated TaO_4[75]
1.0 mol % Ta/xerogel	221, 240 (sh.)	4.9[b]	isolated TaO_4
0.5 mol % Ta/xerogel	221	5.4[b]	isolated TaO_4
Cr compounds			
Cr_2O_3	260, 346, 460, 600, 700 (sh.)	1.8	polymeric CrO_4 chain[91,92]
CrO_3	276, 396, 580−800 (sh.)	1.8	polymeric CrO_4 chain[76,91]
$CoCr_2O_7$	230−280, 348, 424, 485, 612, 659	1.8	dimeric $O_3Cr-O-CrO_3$[41,110]
$K_2Cr_2O_7$	244, 340, 414, 600	1.9	dimeric $O_3Cr-O-CrO_3$[111]
$(NH_4)_2Cr_2O_7$	252, 333, 450	2.4	dimeric $O_3Cr-O-CrO_3$[41,110]
$MgCrO_4$	252, 341, 437	2.5	isolated CrO_4[112]
$(NH_4)_2CrO_4$	252, 341, 418	2.6	isolated CrO_4[113]
K_2CrO_4	244−272, 350, 415	2.8	isolated CrO_4[111,114]
Mo compounds			
α-MoO_3	∼330	3.4	polymeric MoO_5 3D structure[23,115]
$(NH_4)_6Mo_7O_{24}$	320	3.7	cluster, distorted MoO_6[116]
$(NH_4)_2Mo_2O_7$	300	3.8	linear chain of MoO_4/MoO_6[117]
$Al_2(MoO_4)_3$	274	4.2	isolated, distorted MoO_4[118]
$MgMoO_4$	260	4.3	isolated MoO_4[23]
W compounds[119]			
WO_3	267, 328	2.8	polymeric WO_6 3D structure[23,115]
$(NH_4)_6H_2W_{12}O_{40}$	254, 318	3.4	cluster, distorted WO_6[23]
$K_2W_2O_7$	262, 320	3.6	linear chain of WO_4/WO_6[120]
ZrW_2O_8	274	4.0	isolated, distorted WO_4[121]
$Al_2(WO_4)_3$	250	4.2	isolated, distorted WO_4[115]
0.5 mol % W/xerogels	226, 269	4.4[b]	isolated WO_4
Re compounds			
$NaReO_4$, $KReO_4$	238 (sh.), ∼280	3.9−4.0	isolated, distorted ReO_4[23,122]
NH_4ReO_4	238 (sh.), 280	4.0	isolated, distorted ReO_4[23,123]

[a] Eg calculated at elevated temperatures. [b] Eg calculated at room temperature after dehydration.

TABLE 4: Raman and IR Band Positions (cm^{-1}) and UV-vis DRS Eg (eV) Values of Dehydrated Surface Metal Oxide Species on SiO_2 with Their Assignments

assignments	V_2O_5/SiO_2	Nb_2O_5/SiO_2	Ta_2O_5/SiO_2	CrO_3/SiO_2	MoO_3/SiO_2	WO_3/SiO_2	Re_2O_7/SiO_2
υ(M═O)	1038 (s)	980−983 (s)	∼940 (m)	1011 (m)	1020 (m)	1014 (m)	
υ_s(M(═O)$_2$)				982 (s)	976−988 (s)	985 (s)	
υ_{as}(M(═O)$_2$)					965 (m)	968 (w)	
υ_s(M(═O)$_3$)							1010 (s)
υ_{as}(M(═O)$_3$)							977 (m)
υ_s(M−O−Si)	905−925[a] (vw)	915 (vw)		905−910[a] (vw)		900−923[a] (vw)	
υ_s(M−O−M)				576 (vw)			
δ(O−M−O)	340 (w)			396 (w)	364 (w)	346 (w)	343 (w)
Eg (eV)	3.4−3.6 (isolated)	4.2−4.3 (isolated)	5.0−5.2 (isolated)	2.4−2.5 (isolated)	4.0−4.2 (isolated)	4.0−4.2 (isolated)	4.7−4.8 (isolated)

[a] Denotes vibrations also detected with IR spectroscopy.

surface niobia species are present: one that possesses an isolated surface dioxo structure, $(O═)_2Nb(-O-Si)_2$, and one that possesses a dimeric surface monoxo structure, $[(O═Nb)_2O](-O-Si)_4$ with two anchoring Nb−O−Si bonds from each Nb atom.[84] These measurements, however, were actually conducted under ambient conditions where hydrated monoxo Nb_6O_{19} clusters are known to exist.[19,39] The dehydrated surface niobia species on silica, therefore, possess the monoxo surface $O═Nb(-O-Si)_3$ structure.

Supported Ta_2O_5/SiO_2. The dehydrated surface TaO*x* species on SiO_2 are also isolated species (high Eg value from UV−vis DRS) below the maximum dispersion limit. Although the surface TaO*x* species on SiO_2 does not give rise to detectable Raman bands against the stronger bands of the SiO_2 support, the Raman band for the surface TaO*x* species on other oxide supports is found at ∼940 cm^{-1}.[40] The 940 cm^{-1} position is only in agreement with monoxo surface Ta═O species (see Table 1). In situ XANES measurements have shown that the dehydrated

surface TaO*x* species possess TaO_4 coordination.[40,75,85] It has also been proposed that an IR band at 3680 cm^{-1} is related to a Ta−OH functionality.[86] This characterization study, however, did not confirm that crystalline Ta_2O_5 NPs or chemisorbed moisture were absent during the IR measurement. Thus, the dehydrated surface tantala species possess the monoxo O═Ta-(−O−Si)$_3$ structure.

4.2. Molecular Structures of the Dehydrated Group 6 Surface Metal Oxides on Silica. *Supported CrO_3/SiO_2.* The dehydrated surface CrO*x* species on SiO_2 are predominantly present as isolated species (high Eg value from UV−vis DRS). Two distinct isolated surface CrO*x* species, however, are present on the SiO_2 support (see Table 1): dioxo (O═)$_2$Cr(−O−Si)$_2$ (major Raman band at 982 cm^{-1}) and monoxo O═Cr(−O−Si)$_4$ (major Raman band at 1011 cm^{-1}). It should be pointed out that a dioxo O═Cr═O structure should also gives rise to a weak Raman asymmetric stretch at ∼1010 cm^{-1}, but this weak asymmetric band is apparently overshadowed by the strong Raman band of the surface monoxo Cr═O species at 1011 cm^{-1}.

The molecular structural determination of the dehydrated surface CrO*x* species on SiO_2 has received much emphasis in recent years because of the industrial importance of this catalyst system. Early in situ Raman spectroscopy studies of supported CrO_3/SiO_2 catalysts with visible laser excitation (400−700 nm) only detected a single Cr═O band at ∼986 cm^{-1} that were initially assigned to a surface monoxo Cr═O structure on the basis of the lack of observation of an asymmetric stretch mode.[41,42,87] Subsequent studies, however, assigned the vibration to a surface dioxo Cr(═O)$_2$ structure because of agreement with the band positions of gas-phase dioxo CrO_2Cl_2 and CrO_2Br_2 reference compounds.,[88−90] The corresponding IR vibration of the surface CrO*x* species in the ∼980−990 cm^{-1} region, unfortunately, is difficult to observe against the strong SiO_2 IR absorption in this region.[44] An IR band at ∼905 cm^{-1} is observed and has been assigned to the bridging Cr−O−Si vibration (see Supporting Information, Figure S8).[41] Dines and Inglis employed resonance Raman spectroscopy, with 476.5 nm excitation, and observed Raman bands at 990 and 1004 cm^{-1} that they assigned to dioxo ν_s(O═Cr═O) and ν_{as}(O═Cr═O) stretches, respectively, on the basis of ab initio DFT calculations.[31] Groppo et al. also collected resonance Raman spectra, with 442 nm excitation, of CrO*x*−silica aerogels and found well-resolved bands at 987 and ∼1014 cm^{-1} that were also assigned to the dioxo symmetric and asymmetric stretches, respectively.[35,91] More recently, however, Stiegman et al. employed polarized Raman spectroscopy to investigate Cr−silica xerogels and found that there was a large polarization ratio variation between both bands suggesting that the shoulder at ∼1004 cm^{-1} cannot be assigned to the asymmetric vibration related to the ∼986 cm^{-1} band.[47] In agreement with the present study, the 1014 cm^{-1} Raman band does not appear to be related to the asymmetric vibration of the dioxo O═Cr═O species since the two bands reduce independently. All recent Raman studies do agree that the ∼982−987 cm^{-1} Raman band arises from the dehydrated isolated dioxo (O═)$_2$Cr(−O−Si)$_2$ species.

The presence of the three LMCT transitions for the in situ UV−vis DRS of dehydrated supported CrO_3/SiO_2 catalysts at all loading levels (∼250, 340, and 460 nm; see Figure 12) has also led to inconsistent assignments of these LMCT bands in the literature. Weckhuysen et al. summarized the broad range of charge transfer for isolated chromate species (244−277 and 333−370 nm), charge transfer of polychromate species (244−277, 333−370, and 435−476 nm), and d−d transitions of pseudo-octahedral Cr^{+3} including Cr_2O_3 species (586−666 nm).[92] From these assignments, it was proposed that isolated and dimerized surface tetrahedral species are present for over dehydrated supported 0.2 wt % Cr/SiO_2 and that surface polychromate and Cr_2O_3 species also form at increased Cr loadings.[76,88,91] Stiegman et al. also observed the same LMCT transitions at 241, 332, and 450 cm^{-1} for an extremely dilute CrO*x* loading of 0.005 mol % Cr−silica xerogel where only isolated chromate species are present.[47] The current in situ UV−vis DRS Eg values are also consistent with isolated chromia structures (see Tables 2 and 3). There is still some difficulty in completely and properly assigning the UV−vis DRS LMCT transitions for the dehydrated surface chromia species on SiO_2 because of the broad nature of the overlapping bands that prevent distinguishing between surface isolated monoxo and surface isolated dioxo species.

Supported MoO_3/SiO_2. The dehydrated surface MoO*x* species on SiO_2 are present as isolated species (high Eg value from UV−vis DRS). Two distinct surface MoO*x* species are also found to be present on SiO_2 (see Table 1): dioxo (O═)$_2$Mo-(−O−Si)$_2$ (Raman bands at 976−991 cm^{-1} (υ_s) and 965 cm^{-1} (υ_{as})) and monoxo O═Mo(−O−Si)$_4$ (Raman band at 1020 cm^{-1}).

The literature assignments for the surface MoO*x* vibrations from dehydrated supported MoO_3/SiO_2 catalysts have not been consistent. Most of the earlier publications employed IR, Raman, and extended X-ray absorption fine structure/X-ray absorption near edge structure (EXAFS/XANES) spectroscopy to characterize the dehydrated surface MoO*x* structure on SiO_2 and concluded that a surface monoxo structure, with ν_s(Mo═O) vibration at 980−990 cm^{-1}, having either distorted MoO_4, MoO_5, or MoO_6 coordination is present.[93−98] Desiken et al. proposed a surface dioxo (O═)$_2$Mo(−O)$_2$ species based on the Raman band at 955 cm^{-1} with excitation at 647 nm.[99] The very low value of this Raman band and its coincidence with the vibrational band of the hydrated Mo_7O_{24} cluster at ∼950−960 cm^{-1} suggests that the sample was hydrated during these measurements.[23] Iwasawa et al. assigned the dehydrated surface MoO*x* species on SiO_2 to a dimeric surface monoxo structure, proposed as [(O═ Mo)$_2$O](−O−Si)$_4$ with two anchoring Mo−O−Si bonds from each Mo atom, based on EXAFS analysis.[100] Unfortunately, these EXAFS studies were also conducted under ambient conditions where monoxo hydrated Mo_7O_{24} clusters are known present on SiO_2. More recently, Oyama et al. combined Raman (Mo═O vibration present at 984 cm^{-1}) and X-ray absorption spectroscopy (XAS) analysis and concluded that an isolated dioxo surface (O═)$_2$Mo(−O−Si)$_2$ dehydrated structure was present, which was also the basis for theoretical ab initio calculations.[101] The resulting optimized ab initio calculations from various MoO_3/SiO_2 structural models, however, were ambiguous since the calculated Mo═O vibrations were spread over a wide range (893−1008 cm^{-1}). Bell et al. recently predicted the vibrations of isolated surface dioxo MoO_4 and monoxo MoO_5 species attached to a four-silica ring from DFT calculations and obtained the following vibrations for dioxo O═Mo═O (995 (υ_s)/977 (υ_{as}) cm^{-1}) and monoxo Mo═O (1014−1017 cm^{-1}) species.[32] These new DFT vibrational values are in excellent agreement with the current experimental observations and also anticipate the presence of the asymmetric stretch for dioxo species, which was not observed in earlier Raman studies with 514−532 nm excitation.

Supported WO_3/SiO_2. The dehydrated surface WO*x* species on SiO_2 are present as isolated surface species (high Eg value from UV−vis DRS) below the maximum dispersion limit. Two distinct surface WO*x* species are also found to be present on

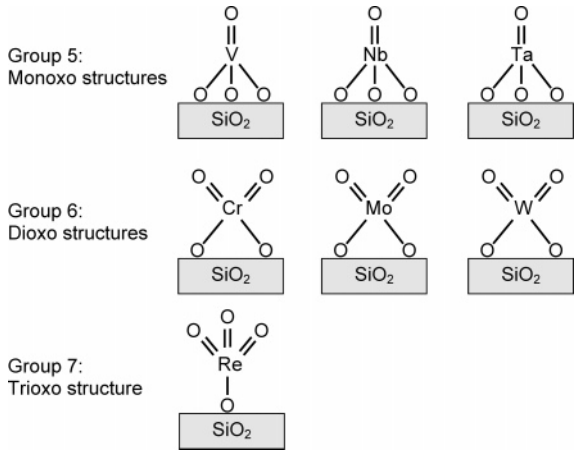

Figure 14. Dehydrated molecular structures of the dominant isolated, surface MO_4 species on silica of supported group 5, 6, and 7 metal oxide catalysts.

SiO_2 (see Table 1): dioxo $(O{=})_2W(-O-Si)_2$ (Raman bands at 985 cm^{-1} (υ_s) and 968 cm^{-1} (υ_{as})) and monoxo $O{=}W(-O-Si)_4$ (Raman band at 1014 cm^{-1}). The relative concentration of the two surface WO_x species varies with temperature with the dioxo structure favored at elevated temperatures. Earlier in situ Raman studies of dehydrated supported WO_3/SiO_2 catalysts only reported the main Raman band at ~975−983 cm^{-1} and assigned this band to isolated monoxo WO_5/WO_6 species[44] since the corresponding asymmetric bands of a dioxo O=W=O structure were not detected. This is the first time that in situ UV−vis spectra of dehydrated supported WO_3/SiO_2 catalysts are reported.

4.3. Molecular Structures of the Dehydrated Group 7 Surface Metal Oxides on Silica. *Supported Re_2O_7/SiO_2.* The dehydrated surface ReO_x species on SiO_2 are present as isolated surface ReO_4 species (high Eg value from UV−vis DRS), and the Raman bands at 1010 and 977 cm^{-1} coincide with that of trioxo $Re(=O)_3$ species (see Table 1). From the in situ Raman and UV−vis spectroscopic measurements, it is concluded that the surface ReO_x species are only present as isolated surface $(O{=})_3Re-O-Si$ sites on the silica support below the maximum dispersion limit. The current in situ Raman findings and conclusions are in agreement with previous publications on dehydrated supported Re_2O_7/SiO_2 catalysts.[45,46] The isolated nature of the dehydrated surface ReO_x species on SiO_2 is confirmed for the first time with in situ UV−vis DRS.

5. Conclusions

The structures of the surface MO_x species present in dehydrated SiO_2 supported group 5−7 metal oxides have been determined with combined in situ Raman, IR, and UV−vis spectroscopic characterization in different environments (oxidizing, reducing, H_2O, and D_2O). All of the dehydrated surface MO_x species on SiO_2 are essentially present as isolated MO_4 species, with the exception of some minor MO_5 species for the group 6 metal oxides. The dehydrated surface MO_4 species possess M=O oxo bonds, and the number of oxo bonds varies with the group number or oxidation state. The group 5 surface metal oxides consist of monoxo structures; the group 6 surface metal oxides primarily possess dioxo structures, and the group 7 surface metal oxide represented by rhenia contains a trioxo structure. Minor amounts of surface monoxo species are also present for the dehydrated group 6 surface metal oxide species on SiO_2. In the case of supported WO_3/SiO_2, comparable amounts of dioxo and monoxo surface WO_4 species are present, and their ratio is a function of temperature. These molecular and electronic structural insights for dehydrated silica-supported metal oxide catalysts will facilitate the establishment of fundamental structure−activity relationships in future catalytic studies.

Acknowledgment. Funding was provided by the U.S. Department of Energy, Basic Energy Sciences (Grant DE-FG02-93ER14350). The silica xerogel samples were kindly provided by Professor A. Stiegman (Florida State University), and we also gratefully appreciate his helpful discussions. We thank Professor R. Wiley (Northeastern University), colleagues, and students for the collaborative work with the IR. We also thank our colleagues in the Operando Molecular Spectroscopy and Catalysis Laboratory, as well as Professors G. Deo (Indian Institute of Technology, Kanpur, India) and J.-M. Jehng (National Chung-Hsing University, Taiwan) and Dr. X. Gao (BASF) for assistance and discussions.

Supporting Information Available: Various Raman, UV-vis DRS, and IR spectra. This material is available free of charge via the Internet at http://pubs.acs.org.

References and Notes

(1) Wachs, I. E.; Segawa, K. In *Characterization of Catalytic Materials*; Wachs, I. E., Ed.; Butterworth-Heinemann: Boston, MA; 1992; pp 69−88.
(2) Wachs, I. E. *Catal. Today* **2005**, *100*, 79.
(3) Wachs, I. E. *Catal. Today* **1996**, *27*, 437.
(4) De Boer, M.; Van Dillen, A. J.; Koningsberger, D. C.; Geus, J. W; Vuurman, M. A.; Wachs, I. E. *Catal. Lett.* **1991**, *11*, 227.
(5) Oyama, S. T.; Somorjai, G. A. *J. Phys. Chem.* **1990**, *94*, 5022.
(6) Oyama, S. T.; Middlebrook, A. M.; Somorjai, G. A. *J. Phys. Chem.* **1990**, *94*, 5029.
(7) Erdohelyi, A.; Solymosi, F. *J. Catal.* **1990**, *123*, 31.
(8) Owens, L.; Kung, H. H. *J. Catal.* **1993**, *144*, 202.
(9) Le Bars, J.; Vedrine, J. C.; Auroux, A.; Trautmann, S.; Baerns, M. *Appl. Catal. A* **1992**, *88*, 179.
(10) Hogan, J. P.; Barks, R. L. Belgium Patent 53067, 1955.
(11) Hogan, J. P.; Norwood, D. D.; Ayres, C. A. *J. Appl. Polym. Sci.* **1981**, *36*, 49.
(12) Thomas, C. L. *Catalytic Processes and Proven Catalysis;* Academic Press: New York, 1970.
(13) Spencer, N. D.; Pereira, C. J.; Grasselli, R. K. *J. Catal.* **1990**, *126*, 546.
(14) Banares, M. A.; Fierro J. L. G.; Moffat, J. B. *J. Catal*. **1993**, *142*, 406.
(15) Mel, J. C.; Moulijn, J. A. In *Catalysis: Science and Technology*; Anderson, J. R., Boudart, M., Eds.; Springer-Verlag: Heidelberg, Germany, 1987; Vol. 8, p 69.
(16) Roark, R. D.; Kohler, S. D.; Ekerdt, J. G.; Kim, D. S.; Wachs, I. E. *Catal. Lett.* **1992**, *16*, 77.
(17) Roark, R. D.; Kohler, S. D.; Ekerdt, J. G. *Catal. Lett.* **1992**, *16*, 71.
(18) Castillo, R.; Koch, B.; Ruiz, P.; Delmon, B. *J. Catal.* **1996**, *161*, 524.
(19) Jehng, J. M.; Wachs, I. E. *Chem. Mater.* **1991**, *3*, 100.
(20) Busca, G.; Ramis, G.; Lorenzelli, V. *J. Mol. Catal.* **1989**, *50*, 231.
(21) Davydov, A. In *Molecular Spectroscopy of Oxide Catalyst Surfaces*; Sheppard, N. T., Ed.; Wiley: Hoboken, NJ, 2003.
(22) Haber, J. Crystallography of Catalyst Types. In *Catalysis: Science and Technology*; Boudart, M., Anderson, J. R., Eds.; Springer-Verlag: Heidelberg, Germany, 1981; Vol. 2, pp 13−95.
(23) Wachs, I. E. Molecular Structures of Surface Metal Oxide Species: Nature of Catalytic Active Sites in Mixed Metal Oxides. In *Metal Oxides: Chemistry and Applications*; Fierro, J. L. G., Heinemann, H., Eds.; CRC Taylor & Francis Press: Boca Raton, FL, 2005.
(24) Busca, G. *J. Raman Spectrosc.* **2002**, *33*, 348.
(25) Weckhuysen, B. M.; Jehng, J. M.; Wachs, I. E. *J. Phys. Chem. B* **2000**, *104*, 7382.
(26) Nakka, L; Wachs, I. E., to be published.
(27) Feher, F. J., unpublished.
(28) Das, N.; Eckert, H.; Hu, H.; Wachs, I. E.; Walzer, J. F.; Feher, F. J. *J. Phys. Chem.* **1993**, *97*, 8240.
(29) Dobler, J.; Pritzsche, M.; Sauer, J. *J. Am. Chem. Soc.* **2005**, *127*, 10861.

(30) Magg, N.; Immaraporn, B.; Giorgi, J. B.; Schroeder, T.; Baumer, M.; Dobler, J.; Wu, Z.; Kondratenko, E.; Cherian, M.; Baerns, M.; Stair, P. C.; Sauer, J.; Freund, H. J. *J. Catal.* **2004**, *226*, 88.

(31) Dines, T. J.; Inglis, S. *Phys. Chem. Chem. Phys.* **2003**, *5*, 1320.

(32) Chempath, S.; Zhang, Y.; Bell, A. T. *J. Phys. Chem. C* **2007**, *111*, 1291.

(33) Tian, H.; Wachs, I. E.; Briand, L. E. *J. Phys. Chem. B* **2005**, *109*, 23491.

(34) Mestl, G.; Srinivasan, T. K. K.; Knozinger, H. *Langmuir* **1995**, *11*, 3795.

(35) Groppo, E.; Damin, A.; Bonino, F.; Zecchina, A.; Bordiga, S.; Lamberti, C. *Chem. Mater.* **2005**, *17*, 2019.

(36) Gao, X.; Bare, S. R.; Weckhuysen, B. M.; Wachs, I. E. *J. Phys. Chem. B* **1998**, *102*, 10842, and references therein.

(37) Jehng, J. M.; Wachs, I. E. *J. Phys. Chem.* **1991**, *95*, 7373.

(38) Gao, X.; Bare, S. R.; Fierro, J. L. G.; Banares, M. A.; Wachs, I. E. *J. Phys. Chem. B* **1998**, *102*, 5653.

(39) Gao, X.; Wachs, I. E.; Wong, M. S.; Ying, J. Y. *J. Catal*. **2001**, *203*, 18.

(40) Chen, Y.; Fierro, J. L. G.; Tanaka, T.; Wachs, I. E. *J. Phys. Chem. B* **2003**, *107*, 5243.

(41) Vuurman, M. A.; Wachs, I. E.; Stufkens, D. J.; Oskam, A. *J. Mol. Catal*. **1993**, *80*, 209.

(42) Kim, D. S.; Tatibouet, J. M.; Wachs, I. E. *J. Catal.* **1992**, *136*, 209.

(43) Kim, D. S.; Wachs, I. E.; Segawa, K. *J. Catal.* **1994**, *146*, 268.

(44) Kim, D. S.; Ostomecki, M.; Wachs, I. E.; Kohler, S. D.; Ekerdt, J. G. *Catal. Lett.* **1995**, *33*, 209.

(45) Vuurman, M. A.; Stufkens, D. J.; Oskam., A. *J. Mol. Catal*. **1992**, *76*, 263.

(46) Kim, D. S.; Wachs, I. E. *J. Catal.* **1993**, *141*, 419.

(47) Moisii, C.; Deguns, E. W.; Lita, A.; Callahan, S. D.; van de Burgt, L. J.; Magana, D.; Stiegman, A. E. *Chem. Mater.* **2006**, *18*, 3965.

(48) Moisii, C.; Curran, M. D.; van de Burgt, L. J.; Stiegman, A. E. *J. Mater. Chem.* **2005**, *15*, 3519.

(49) (a) Burcham, L. J.; Briand, L. E.; Wachs, I. E. *Langmuir* **2001**, *17*, 6164. (b) Li, W.; Willey, R. J. *J. Non-Cryst. Solids* **1997**, *212*, 243.

(50) Weber, R. S. *J. Catal.* **1995**, *151*, 470.

(51) Brinker, C. J.; Kirkpatrick, R. J.; Tallant, D. R.; Bunker, B. C.; Montez, B. *J. Non-Cryst. Solids* **1988**, *99*, 418.

(52) McMillan, P. *Am. Mineral.* **1984**, *69*, 622.

(53) Galeener, F. L.; Mikkelsen, J. C., Jr. *Phys. Rev. B* **1981**, *23*, 5527.

(54) Galeener, F. L.; Geissberger, A. E. *Phys. Rev. B* **1983**, *27*, 6199.

(55) Morrow, B. A.; Mcfarlan, A. J. *J. Non-Cryst. Solids* **1990**, *120*, 61.

(56) Uchino, T.; Tokuda, Y.; Yoko, T. *Phys. Rev. B* **1998**, *58*, 5322.

(57) Vansant, E. F.; Voort, P. V. D.; Vrancken, K. C. *Stud. Surf. Sci. Catal.* **1995**, *93*.

(58) Eckert, H.; Wachs, I. E. *J. Phys. Chem.* **1989**, *93*, 6796.

(59) Oyama, S. T.; Went, G. T.; Lewis, K. B.; Bell, A. T.; Somorjai, G. A. *J. Phys. Chem.* **1989**, *93*, 6786.

(60) Resini, C.; Montanari, T.; Busca, G.; Jehng, J. M.; Wachs, I. E. *Catal. Today* **2005**, *99*, 105.

(61) Banares, M. A.; Cardoso, J. H.; Agullo-Rueda, F.; Correa-Bueno, J. M.; Fierro, J. L. G. *Catal. Lett.* **2000**, *64*, 191.

(62) Burcham, L. J.; Deo, G.; Gao, X.; Wachs, I. E. *Topics Catal.* **2000**, *11/12*, 85.

(63) Went, G. T.; Oyama, S. T.; Bell, A. T. *J. Phys. Chem.* **1990**, *94*, 4240.

(64) Deo, G.; Wachs, I. E., *J. Catal.* **1994**, *146*, 323.

(65) Avdeev, V. I.; Zhidomirov, G. M. *Res. Chem. Intermed.* **2004**, *30*, 41.

(66) Burcham, L. J.; Datka, J.; Wachs, I. E. *J. Phys. Chem. B* **1999**, *103*, 6015.

(67) Maurer, S. M.; Ko, E. I. *J. Catal.* **1992**, *135*, 125.

(68) Huuhtanen, J.; Sanati, M.; Andersson, A.; Andersson, S. L. T. *Appl. Catal. A* **1993**, *97*, 197.

(69) Baltes, M.; Kytokivi, A.; Weckhuysen, B. M.; Schoonheydt, R. A.; van der Voort, P.; Vansant, E. F. *J. Phys. Chem. B* **2001**, *105*, 6211.

(70) Szanics, J.; Okubo, T.; Kakihana, M. *J. Alloys Compd.* **1998**, *281*, 206.

(71) Kim, D. S.; Wachs, I. E. *J. Catal.* **1993**, *142*, 166.

(72) Yamashita, H.; Anpo, M. *Curr. Opin. Solid State Mater. Sci.* **2003**, *7*, 471.

(73) Banares, M. A., private communication.

(74) Ramis, G.; Cristiani, C.; Elmi, A. S.; Villa, P. L.; Busca, G. *J. Mol. Catal.* **1990**, *61*, 319.

(75) Jehng, J.-M.; Tung, W.-C.; Huang, C.-H.; Wachs, I. E. *Microporous Mesoporous Mater.* **2007**, *99*, 299.

(76) Amano, F.; Yamahuchi, T.; Tanaka, T. *J. Phys. Chem. B* **2006**, *110*, 281.

(77) (a) Banares, M. A.; Wachs, I. E. *J. Raman Spectrosc.* **2002**, *33*, 359. (b) Banares, M. A.; Martinez-Huerta, M.; Gao, X.; Wachs, I. E.; Fierro, J. L. G. *Stud. Surf. Sci. Catal.* **2000**, *130D*, 3125.

(78) Nguyen, L. D.; Loridant, S.; Launay, H.; Pigamo, A.; Dubois, J. L.; Millet, J. M. M. *J. Catal.* **2006**, *237*, 38.

(79) Berndt, H.; Martin, A.; Bruckner, A.; Schreier, E.; Muller, D.; Kosslick, H.; Wolf, G. U.; Lucke, B. *J. Catal.* **2000**, *191*, 384.

(80) Schraml-Marth, M.; Wokaun, A.; Pohl, M.; Krauss, H.-L. *J. Chem. Soc., Faraday Trans.* **1991**, *87*, 2635.

(81) Van Der Voort, P.; White, M. G.; Mitchell, M. B., Verberckmoes, A. A.; Vansant, E. F. *Spectrochim. Acta A* **1997**, *53*, 2181.

(82) Baltes, M.; Cassiers, K.; Van der Voort, P.; Weckhuysen, B. M.; Schoonheydt, R. A.; Vansant, E. F. *J. Catal.* **2001**, *197*, 160.

(83) Keller, D. E.; de Groot, F. M. F.; Koningsberger, D. C.; Weckhuysen, B. M. *J. Phys. Chem. B* **2005**, *109*, 10223.

(84) (a) Ichikuni, N.; Shirai, M.; Iwasawa, Y. *Catal. Today* **1996**, *28*, 49. (b) Iwasawa, Y. Characterization and Chemical Design of Oxide Surfaces. *Stud. Surf. Sci. Catal.* J. W. Hightower, J. W., Delgass, W. N., Iglesia, E., Bell, A. T., Eds.; Proceedings of the 11th International Cong. Catal. 1996; Vol. 101, pp 21−34.

(85) Tanaka, T.; Nojima, H.; Yamamoto, T.; Takenaka, S.; Funabiki, T.; Yoshida, S. *Phys. Chem. Chem. Phys.* **1999**, *1*, 5235.

(86) Ushikubo, T.; Wada, K. *J. Catal.* **1994**, *148*, 138.

(87) Weckhuysen, B. M.; Wachs, I. E. *J. Phys. Chem. B* **1996**, *100*, 14437.

(88) Weckhuysen, B. M.; Schoonheydt, R. A.; Jehng, J. M.; Wachs, I. E.; Cho, F. J.; Ryoo, R.; Kijlstra, S.; Poels, E. *J. Chem. Soc., Faraday Trans.* **1995**, *91*, 3245.

(89) Jehng, J.-M.; Wachs, I. E.; Weckhuysen, B. M. Schoonheydt, R. A. *J. Chem. Soc., Faraday Trans.* **1995**, *91*, 953.

(90) Hardcastle, F. D.; Wachs, I. E. *J. Mol. Catal.* **1988**, *46*, 173.

(91) Groppo, E.; Lamberti, C.; Bordiga, S.; Spoto, G.; Zecchina, A. *Chem. Rev.* **2005**, *105*, 115.

(92) Weckhuysen, B. M.; Wachs, I. E.; Schoonheydt, R. A. *Chem. Rev.* **1996**, *96*, 3327.

(93) Cornac, M.; Janin, A.; Lavalley, J. C. *Polyhedron* **1986**, *5*, 183.

(94) Williams, C. C.; Ekerdt, J. G.; Jehng, J.-M.; Hardcastle, F. D.; Turek, A. M.; Wachs, I. E. *J. Phys. Chem.* **1991**, *95*, 8781.

(95) Hu, H.; Bare, S. R.; Wachs, I. E. *J. Phys. Chem.* **1995**, *99*, 10897.

(96) Banares, M. A.; Hu, H.; Wachs, I. E. *J. Catal.* **1994**, *150*, 407.

(97) Zhang, W.; Desikan, A.; Oyama, S. T. *J. Phys. Chem.* **1995**, *99*, 14468.

(98) Ohler, N.; Bell, A. T. *J. Phys. Chem. B* **2005**, *109*, 23419.

(99) Desikan, A. N.; Huang, L.; Oyama, S. T. *J. Phys. Chem.* **1991**, *95*, 10050.

(100) Iwasawa, Y.; Asakura, K.; Ishii, H.; Kuroda, H. *Z. Phys. Chem.* **1985**, *144*, 105.

(101) Radhakrishnan, R.; Reed, C.; Oyama, S. T.; Seman, M.; Kondo, J. N.; Domen, K.; Ohminami, Y.; Asakura, K. *J. Phys. Chem. B* **2001**, *105*, 8519.

(102) Nakamoto, K. *Infrared and Raman Spectra of Inorganic and Coordination Compounds*, 4th ed; Wiley: New York, 1986; pp 140−149 and references therein.

(103) Cieslak-Golonka, M. *Coord. Chem. Rev.* **1991**, *109*, 223.

(104) Stammreich, H.; Kawai, K.; Tavares, Y. *Spectrochim. Acta* **1959**, *15*, 438.

(105) Muller, A.; Schmidt, K. H.; Ahlborn, E.; Lock, C. J. L. *Spectrochim. Acta A* **1973**, *29*, 1773.

(106) Nakamoto, K. *Infrared and Raman Spectra of Inorganic and Coordination Compounds*, 4th ed; Wiley: New York, 1986; pp 157 and references therein.

(107) (a) Muller, A.; Krebs, B.; Hoeltje, W. *Spectrochim. Acta* **1967**, *23*, 2753. (b) Beattie, I. R.; Crocombe, R. A.; Ogden, J. S. *J. Chem. Soc., Dalton Trans.* **1977**, 1481.

(108) Wachs, I. E.; Chen, Y.; Jehng, J. M.; Briand, L. E.; Tanaka, T. *Catal. Today* **2003**, *78*, 13.

(109) (a) Tealdi, C.; Ialam, M. S.; Malavasi, L.; Flor, G. *J. Solid State Chem.* **2004**, *177*, 4359. (b) Sun, D. C.; Senz, S.; Hesse, D. *J. Eur. Ceram. Soc.* **2004**, *24*, 2453.

(110) Mattes, R. Z. *Z. Anorg. Allg. Chem.* **1971**, *382*, 163.

(111) Pandya, K. I. *Phys. Rev. B* **1994**, *50*, 15509.

(112) Bertrand, G.; Dusausoy, Y.; Protas, J.; Watelle-Marion, G. *C. R. Acad. Sci. Paris, Ser. C* **1971**, *272*, 530.

(113) Stephens, J. S.; Cruickshank, D. W. J. *Acta Cryst. B* **1970**, *26*, 437.

(114) Adams, D. M.; Hooper, M. A.; Lloyd, M. H. *J. Chem. Soc. A* **1971**, 946.

(115) Wells, A. *Structural Inorganic Chemistry;* Oxford University: London, 1984.

(116) Greenwood, N. N.; Earnshaw, A. *Chemistry of the Elements;* Pergamon Press: Elmsford, NY, 1989.

(117) (a) Knopnadel, I.; Hartl, H.; Hunnius, W. D.; Fuchs, J. *Angew. Chem.* **1974**, *86*, 894. (b) Hove, A. R.; Bildsoe, H.; Skibsted, J.; Brorson, M.; Jakobsen, H. J. *Inorg. Chem.* **2006**, *45*, 10873.
(118) Hardcastle, F. D.; Wachs, I. E. *J. Raman Spectrosc.* **1990**, *21*, 683.
(119) Ross, E. I.; Wachs, I. E., to be published.
(120) Becher, H. J. *Z. Anorg. Allg. Chem.* **1981**, *474*, 63.
(121) Jorgensen, J. D.; Hu, Z.; Teslic, S.; Argyriou, D. N.; Short, S.; Evans, J. S. O.; Sleight, A. W. *Phys. Rev. B* **1999**, *59*, 215.
(122) (a) Spitaler, J.; Ambrosch-Draxl, C.; Nachbaur, E.; Belaj, F.; Gomm, H.; Netzer, F. *Phys. Rev. B* **2003**, *67*, 115127. (b) Lock, C. J. L.; Turner, G. *Acta Cryst.* **1975**, *B31*, 1764. (c) Pendharkar, A. V.; Mande, C. *Pramana* **1973**, *1*, 104.
(123) Swainson, I. P.; Brown, R. J. C. *Acta Cryst.* **1997**, *B53*, 76.